





Simulating Hail and Lightning Over the Alpine Adriatic Region—A Model Intercomparison Study

Journal Article

Author(s):

Malečić, Barbara; Cui, Ruoyi ; Demory, Marie-Estelle ; Horvath, Kristian; Jelić, Damjan; Schär, Christoph ; Telišman Prtenjak, Maja; Velasquez Alvarez, Patricio Andres ; Ban, Nikolina

Publication date:

2023-07-16

Permanent link:

<https://doi.org/10.3929/ethz-b-000623402>

Rights / license:

[Creative Commons Attribution-NonCommercial 4.0 International](#)

Originally published in:

Journal of Geophysical Research: Atmospheres 128(13), <https://doi.org/10.1029/2022JD037989>

Funding acknowledgement:








180587 - Severe Weather over the Alpine-Adriatic region in a Changing Climate (SWALDRIC) (SNF)



RESEARCH ARTICLE

10.1029/2022JD037989

Simulating Hail and Lightning Over the Alpine Adriatic Region—A Model Intercomparison Study

B. Malečić¹ , R. Cui² , M. E. Demory^{2,3,4,5} , K. Horvath⁶, D. Jelić¹ , C. Schär² ,
M. Telišman Prtenjak¹, P. Velasquez² , and N. Ban⁷ 

Key Points:

- Km-scale simulations over the Alpine-Adriatic region show that HAILCAST and Lightning Potential Index are successful in diagnosing observed hail and lightning
- Results are presented using the Consortium for Small Scale Modeling and Weather Research and Forecasting models for a total of eight case studies covering different types of hail storms
- Overall, the two models yield similar results, but some systematic differences are found and tied to differences in model structure

Supporting Information:

Supporting Information may be found in the online version of this article.

Correspondence to:

B. Malečić,
barbara.malecic@gfz.hr

Citation:

Malečić, B., Cui, R., Demory, M. E., Horvath, K., Jelić, D., Schär, C., et al. (2023). Simulating hail and lightning over the Alpine Adriatic region—A model intercomparison study. *Journal of Geophysical Research: Atmospheres*, 128, e2022JD037989. <https://doi.org/10.1029/2022JD037989>

Received 7 OCT 2022

Accepted 8 JUN 2023

Author Contributions:

Conceptualization: M. E. Demory, K. Horvath, C. Schär, M. Telišman Prtenjak, N. Ban

Data curation: R. Cui, D. Jelić, P. Velasquez

Formal analysis: B. Malečić

Investigation: B. Malečić

Methodology: B. Malečić, R. Cui, M. E. Demory, N. Ban

Project Administration: C. Schär, M. Telišman Prtenjak, N. Ban

¹Faculty of Science, Department of Geophysics, University of Zagreb, Zagreb, Croatia, ²Institute for Atmospheric and Climate Science, ETH Zurich, Zurich, Switzerland, ³Wyss Academy for Nature, University of Bern, Bern, Switzerland, ⁴Climate and Environmental Physics, Physics Institute, University of Bern, Bern, Switzerland, ⁵Oeschger Centre for Climate Change Research, University of Bern, Bern, Switzerland, ⁶Croatian Meteorological and Hydrological Service, Zagreb, Croatia, ⁷Department of Atmospheric and Cryospheric Sciences, University of Innsbruck, Innsbruck, Austria

Abstract Hail is a significant convective weather hazard, often causing considerable crop and property damage across the world. Although extremely damaging, hail still remains a challenging phenomenon to model and forecast, given the limited computational resolution and the gaps in understanding the processes involved in hail formation. Here, eight hailstorms occurring over the Alpine-Adriatic region are analyzed using simulations with the Weather Research and Forecasting (WRF) and the Consortium for Small Scale Modeling (COSMO) models, with embedded HAILCAST and Lightning Potential Index (LPI) diagnostics at kilometer-scale grid spacing (~2.2 km). In addition, a systematic model intercomparison study is performed to investigate the ability of the different modeling systems in reproducing such convective extremes, and to further assess the uncertainties associated with simulations of such localized phenomena. The results are verified by hailpad observations over Croatia, radar estimates of hail over Switzerland, and lightning measurements from the LINET network. The analysis reveals that both HAILCAST and LPI are able to reproduce the affected area and intensities of hail and lightning. Moreover, hail and lightning fields produced by both models are similar, although a slight tendency of WRF to produce smaller hail swaths with larger hailstones and higher LPI compared to COSMO is visible. It is found that these differences can be explained by systematic differences in vertical profiles of microphysical properties and updraft strength between the models. Overall, results are promising and indicate that both HAILCAST and LPI could be valuable tools for real-time forecasting and climatological assessment of hail and lightning in current and changing climate.

Plain Language Summary Hail is a dangerous type of weather that can cause damage to crop and property. In this study, two numerical models are used, the Weather Research and Forecasting (WRF) and the Consortium for Small Scale Modeling (COSMO), to simulate eight hailstorms in the Alpine-Adriatic region. These simulations included two diagnostic tools, HAILCAST and Lightning Potential Index (LPI), to simulate hail and lightning. The simulations were verified by direct measurements of hail, radar estimates of hail, and lightning measurements. The study found that both HAILCAST and LPI were able to accurately predict characteristics of hail and lightning. The models produced similar results, with a slight difference in hail size and LPI between the WRF and COSMO models, which was attributed to differences in microphysical properties and updraft strength. Overall, the study suggests that these diagnostic tools could be useful for real-time forecasting and assessing hail and lightning in the present and future climate.

1. Introduction

Hail is a severe weather hazard that can produce significant crop and property damage across the world (Allen et al., 2020), especially when it occurs over highly populated areas with high-density assets (Kunz et al., 2018). In the literature, a large number of hailstorms causing more than US\$1 billion in damage is reported across the world (Brown et al., 2015; Changnon, 2009; Kunz et al., 2018; Púčík et al., 2019; Schuster et al., 2005). Punge and Kunz (2016) and Púčík et al. (2019) describe several hail hotspots in Europe, including the pre-Alpine and Adriatic areas. Although large hail occurs less often over the highest mountain peaks in the central Alps, severe hailstorms frequently affect Switzerland with up to 4 large hail days per year (Nisi et al., 2016; Púčík et al., 2019). In this area, the maximum hail diameter can in extreme cases even exceed 10 cm (e.g., see Figure 8 from Púčík et al., 2019). Furthermore, parts of Croatia (Jelić et al., 2020; Počakal et al., 2018) and broader northern Adriatic

© 2023 The Authors.

This is an open access article under the terms of the [Creative Commons Attribution-NonCommercial License](https://creativecommons.org/licenses/by-nc/4.0/), which permits use, distribution and reproduction in any medium, provided the original work is properly cited and is not used for commercial purposes.

Resources: K. Horvath, C. Schär, M. Telišman Prtenjak
Software: B. Malečić, R. Cui
Supervision: M. E. Demory, N. Ban
Validation: B. Malečić
Visualization: B. Malečić
Writing – original draft: B. Malečić
Writing – review & editing: B. Malečić, R. Cui, M. E. Demory, K. Horvath, D. Jelić, C. Schär, M. Telišman Prtenjak, P. Velasquez, N. Ban

region (Manzato, 2012) have similar statistics of hail frequency as southern Germany or southeastern Austria (Punge & Kunz, 2016). Therefore, considering the high economic losses associated with (severe) hailstorms, and high frequencies of hail occurrence, it is very important to have reliable hail models, both for short-term numerical weather prediction (NWP) and long-term climate-change adaptation strategies.

One of the largest limitations in understanding processes involved in hail formation is the lack of dense and direct measurements of hail properties on the ground. Hailpads, which are simple meteorological devices consisting of a stand and a measuring plate, represent one of the few methods to detect and measure hailstones directly on the ground. Besides the number of falling hailstones and their diameters, hailpads can also detect the intensity (i.e., kinetic energy) of hail (Smith & Waldvogel, 1989). In Europe, hailpad networks exist in several regions including parts of Spain, France, Greece, northern Italy, eastern Austria and parts of Croatia (Berthet et al., 2011; Dessens, 1998; Giaiotti et al., 2003; Počakal, 2011; Počakal et al., 2009; Sioutas et al., 2009; Svabik, 1989) and have also been used in randomized hail suppression experiments in Switzerland (Federer et al., 1978). Although hailpads are one of the few sources of direct information on hail occurrence, they provide spatially discrete (but unique) information on hail occurrence as they only record hail at the point where they are installed.

Another source of information on hail occurrence is related to weather radars. As the abilities of weather radars to detect different kinds of hydrometeors such as rain, snow and hail progressed over the years, several hail detection algorithms have been developed (e.g., Waldvogel et al., 1979; Witt et al., 1998). At present, hail detection algorithms are widely used as hail proxies and can provide spatially continuous information on various hail properties, for example, probability of hail occurrence or maximum expected hailstone size. In Switzerland, two hail detection algorithms are operational in real-time, namely, Probability of Hail (POH, Foote et al., 2005; Waldvogel et al., 1979) that indicates a probability of a hailstorm occurring at a certain location, and Maximum Expected Severe Hail Size (MESHS, Joe et al., 2004; Treloar, 1998) that estimates expected severe hail size at the ground over the Alpine region.

An additional challenge in understanding hail processes is the limited number of high-resolution modeling studies of hailstorms. With increasing computational power, it has become possible to run simulations at convection-permitting scales (horizontal grid spacing <4 km). Several studies reported the benefits of using models at kilometer scales for more realistic representations of convective processes (Leutwyler et al., 2017), mean diurnal cycles of precipitation (Ban et al., 2014), spatial precipitation patterns and associated extreme values (Brisson et al., 2016, 2018; Fowler et al., 2021; Pichelli et al., 2021; Prein et al., 2013), better representation of convective clouds (Brisson et al., 2016; Hentgen et al., 2019; Keller et al., 2016), short-term heavy precipitation events (Vergara-Temprado et al., 2021) local wind systems like sea breeze (Belušić et al., 2018), and complex terrain winds (Horvath et al., 2012). Since models, when run at km scales, can produce a more realistic representation of convective processes, Adams-Selin and Ziegler (2016) integrated a physically improved 1D hail growth scheme—called HAILCAST (Brimelow et al., 2002; Jewell & Brimelow, 2009; Poolman, 1992)—with the km-scale WRF model. When HAILCAST is coupled with WRF, the model simulates the maximum expected hail size at the ground using the profiles of cloud liquid and ice water, vertical velocity, temperature, water vapor and pressure fields from a given model timestep. Several recent studies employed HAILCAST embedded in high-resolution numerical models, such as WRF or COSMO, to study hailstorms occurring over the United States and Europe. The studies found that the models can reproduce the atmospheric conditions and triggering mechanisms responsible for hailstorm formation, resulting in simulating comparable hailstorms to those observed over the complex terrain of the United States (Adams-Selin et al., 2019; Adams-Selin & Ziegler, 2016), Switzerland (Cui et al., 2023; Raupach et al., 2021; Trefalt et al., 2018), Italy (Manzato et al., 2020; Tiesi et al., 2022), and Croatia (Malečić et al., 2022).

Similar to hail, lightning poses a serious threat to human lives (Curran et al., 2000; Holle et al., 2005), wind turbines (Rachidi et al., 2008) and transportation (Kanata et al., 2012; Lee & Collins, 2017; Thornton et al., 2017). Moreover, lightning is a major cause of wildfires (Abatzoglou & Williams, 2016; Dowdy et al., 2017; Latham & Williams, 2001). Considering the hazards associated with lightning occurrence, the lightning potential index (LPI) was developed as a tool for diagnosing areas prone to lightning discharges (Lynn & Yair, 2010; Yair et al., 2010). With a better representation of convective processes km-scale simulations, LPI offers the possibility to use the parameterizations of lightning that describe the non-inductive process occurring inside a thundercloud (Brisson et al., 2021; Yair et al., 2010). It is defined as a potential for charge formation and separation inside a thundercloud and it relies on the presence of both solid and liquid hydrometeors. Even though LPI is not directly

connected to the observed number of lightning flashes, several studies found that LPI could be a valuable tool for implicit lightning forecasting in the COSMO (Cui et al., 2023; Sokol & Minářová, 2020) and WRF (Lagasio et al., 2017; Malečić et al., 2022; Yair et al., 2010) models. Recently, LPI was used in the climatological assessment of lightning over Germany (Brisson et al., 2021) and proved to be a better indicator of lightning occurrence than the commonly used convective available potential energy times precipitation (CAPE x PREC) parameterization (Romps et al., 2014).

Recently, an effort was made to utilize both HAILCAST and LPI to study hailstorms occurring in Croatia using WRF (Malečić et al., 2022) and over the broader Alpine-Adriatic region using COSMO (Cui et al., 2023) models. More specifically, Cui et al. (2023) selected 8 days with severe convection over the Alpine-Adriatic region based on the observed impacts and underlying synoptic forcing to study the mechanisms responsible for severe weather effects. Adopting the process-oriented approach, the authors found that both HAILCAST and LPI successfully reproduced observed hail and lightning characteristics over a broad range of synoptic situations.

Motivated by the promising results, this study aims to complement the valuable previous research on hailstorm simulation over the topographically complex Alpine-Adriatic region (Figure 1a). More specifically, we employ these two diagnostic tools in km-scale models (COSMO and WRF) to simulate hailstorms analyzed by Cui et al. (2023), with a geographical focus on Croatia and Switzerland. By analyzing eight hail cases using two models, we aim (a) to conduct a systematic and quantitative evaluation of the model's performance for hail and lightning, and (b) to identify the robustness of HAILCAST and LPI results produced by two intrinsically different modeling systems. The outcome of this study reveals information about model biases and the origins of disagreements between the two models in simulating severe storms associated with hail and lightning over the complex Alpine-Adriatic region. Moreover, this study benefits from two valuable but intrinsically different data sets of hail observations, namely spatially discrete in-situ hail measurements from the hailpad network (and two hailpad polygons) in Croatia, and spatially continuous remote-sensing radar estimates on hail occurrence in Switzerland. Therefore, the objectives of this paper can be summarized as follows.

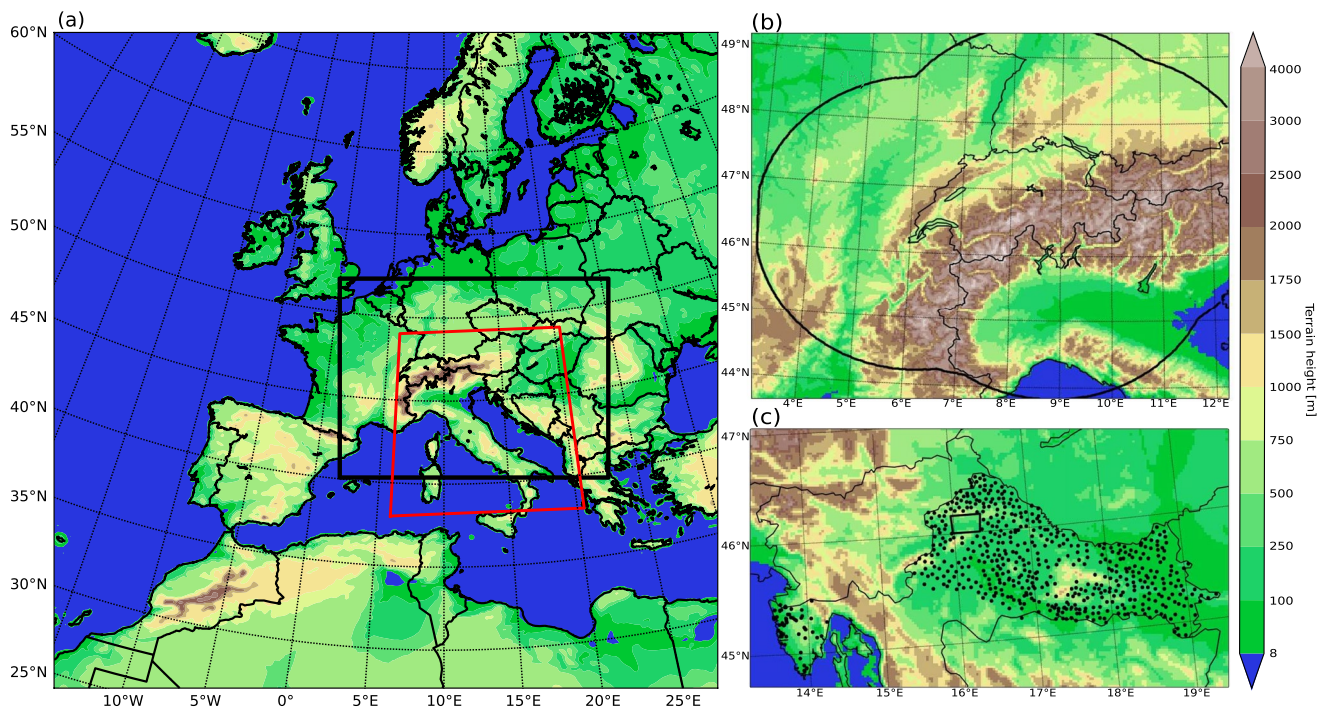


Figure 1. (a) Terrain height (above sea level) as represented in Weather Research and Forecasting (WRF) for the outer 12 km domain. The inner 2.2 km domain is indicated with the black rectangle. The domain where LINET measurements are available is indicated with the red line. (b) Terrain height as represented in WRF for the 2.2 km domain over the Alpine region. The black line indicates the Swiss radar spatial coverage. (c) Terrain height as represented in WRF for the 2.2 km domain over Croatia. The black dots indicate the positions of hailpads.

- To what extent can HAILCAST and LPI credibly diagnose the occurrence of hail and lightning?
- How do simulations with two distinct models but the same diagnostic hail and lightning modules differ from each other?

This paper is organized as follows: Section 2 describes the selected hail events and observational data used to evaluate COSMO and WRF models. An overview of the model setups and evaluation approach is indicated in Section 3. The results are presented and discussed in Section 4. The conclusions and remarks are given in Section 5.

2. Selected Hailstorms and Observational Data

Eight days with severe convection occurring over the Alpine-Adriatic region already analyzed in Cui et al. (2023) are selected for the analysis. Out of eight selected days, hailstorms were observed in Croatia and/or Switzerland during seven of these days. During the day without observed hail in the central and eastern Alps, intense precipitation over the Alps leading to severe flooding is reported. Hailstorms are selected based on their intensity, measured by their impact or the kinetic energy recorded with hailpads. Besides that, an attempt was made to select hailstorms occurring over a set of synoptic and mesoscale situations to assess the abilities of both models to reproduce the observed convection during a variety of driving conditions. Moreover, by selecting a day where no hail is observed, the ability of both models to distinguish between convective days with and without hail is assessed. The type of observations available for eight selected events along with a brief description of their impacts are listed in Table 1.

To assess the model's ability to reproduce the observed severe weather events, several datasets are used. To validate simulated precipitation over the Alpine-Adriatic region, the Final Run of Integrated Multi-satellite Retrievals for Global Precipitation Measurement (IMERG) mission (Huffman et al., 2019) data set is used. IMERG is a globally gridded precipitation product that estimates surface precipitation rates at 0.1° spatial and 30 min temporal resolution. IMERG incorporates satellite microwave precipitation estimates, microwave-calibrated infrared satellite estimates and rain gauge observations. Combining remote sensing and in-situ observations, IMERG provides spatially and temporally continuous and homogeneous precipitation estimates over the whole Alpine-Adriatic region.

Table 1
Selected Convective Events Over the Alpine-Adriatic Region

Date	Observations of hail	Impact
23 July 2009	Radar	A thunderstorm embedded in a cold front hit Switzerland and caused damage of around 261 million CHF.
1 June 2013	No hail observed in Croatia and Switzerland	Intense precipitation over the Alps led to severe flooding in central and eastern Switzerland. The estimated damage is 15 million CHF.
18 June 2013	Radar	Significant damage to vineyards in eastern Switzerland.
25 June 2017	Radar, Hailpads	Large mesoscale convective system observed in Croatia. 74 impacted hailpads with maximum hailstone diameter of 31.4 mm
8 July 2017	Radar	Damage to crops and vineyards in Switzerland.
24 July 2017	Radar, Hailpads	Large hailstones were observed in Croatia. Maximum recorded hailstone diameter is 54.2 mm.
17 May 2018	Hailpads	Non-gradient pressure field over Croatia. Significant kinetic energy and hail size (up to 19.9 mm) in northeastern Croatia.
30 May 2018	Radar	Significant damage to cars and buildings in central and eastern Switzerland.

Note. The type of available observations and a short description of the event's impact is indicated. Radar observations are covering Switzerland while hailpad observations are associated with the hailpad network in Croatia. More information on the impacts of some of these events can be obtained through <http://www.sturmarchiv.ch/index.php/Hagel>.

Further, to assess the ability of LPI to reproduce the observed lightning activity, lightning data from the Lightning Detection Network (LINET) (Betz et al., 2009) is used. With 190 sensors in 31 countries that are up to 250 km away, LINET successfully detects cloud-to-ground and intracloud lightning flashes and differentiates between positive and negative discharges across Europe. Moreover, the LINET network can detect weaker stroke signals with a current amplitude lower than 1 kA. With continuous improvements of the LINET network, the median values of detected current amplitude values had decreased by half from 2009 (Franc et al., 2016), showing significant improvement in the sensitivity detection toward smaller stroke current amplitudes. For most of the European region (Franc et al., 2016; Jelić et al., 2021), the average minimum detectable signal is 0.7 kA, and the median location accuracy error is ± 84 m. Here, we considered total lightning information, that is, we did not differentiate between types or polarities of lightning flashes as LPI presents the overall potential for lightning activity without preferences to the type or polarity of lightning discharges. The total lightning for the examined cases was taken from the 2D database of lightning flashes at a $3 \text{ km} \times 3 \text{ km}$ horizontal and 2 min temporal resolution (developed by Jelić et al., 2021) over the domain shown in Figure 1a.

Next, hail detection products from the Swiss radar network (Germann et al., 2015; Willemse & Furger, 2016) operated by MeteoSwiss are used to assess the HAILCAST results. Namely, the operationally computed POH product is used. POH indicates the grid-based probability of hail reaching the ground. It is computed following Waldvogel et al. (1979) and Foote et al. (2005) from the difference in height between the altitude of the center of the highest radar bin at which 45 dBZ echo (i.e., Echo Top of 45 dBZ) is found and the height of the freezing level retrieved from the forecasts of the operational numerical prediction model COSMO. POH has been verified using insurance loss data (Morel, 2014; Nisi et al., 2016) and a good agreement between hail damage and POH $\geq 80\%$ was found. The area in which this product is available is indicated in Figure 1b.

Finally, HAILCAST results are assessed against in-situ hail measurements from the Croatian hailpad network. It consists of (a) hail suppression stations in the continental region of Croatia, (b) a specially designed hailpad polygon in northwestern Croatia, and (c) hailpad stations in the northeastern (NE) Adriatic region (Figure 1c). Overall, 590 hailpads on hail suppression stations, and 150 hailpads on the polygon, with average spacing between hailpads of ~ 5.5 and ~ 2 km, respectively, have been installed and maintained by the Croatian Meteorological and Hydrological Service (Počakal, 2011; Počakal et al., 2009). Moreover, during the VITCLIC project (<https://www.pmf.unizg.hr/geof/en/research/climatology/vitclic>) 65 hailpads were installed in Istria (NE Adriatic) in the vicinity of an agricultural area with vineyards. Notably, the Istrian region is not a part of the hail suppression network; therefore, hail observations from these hailpads are not under the potential influence of hail suppression activities.

3. Modeling Setup and Evaluation Approach

3.1. COSMO and WRF Setups

Selected hailstorms were simulated using an Advanced Research Weather Research and Forecasting (WRF, version 4.1.5) model (Skamarock et al., 2019), and the climate version of the Consortium for Small Scale Modeling (COSMO-crCLIM based on COSMO 5.0) model (Baldauf et al., 2011; Leutwyler et al., 2017; Schär et al., 2020) alongside HAILCAST and LPI. An attempt was made to make a setup of both models as similar as possible. Additionally, one of the hailstorms is simulated using the newest version of COSMO v6.0 model.

The modeling setup consisted of two one-way nested domains with horizontal grid spacing of approximately 12 km (0.11°) and 2.2 km (0.02°) (Figure 1a). The model setup consists of 65 vertical levels in WRF and 60 vertical levels in COSMO. WRF uses a hybrid sigma-pressure vertical coordinate (Park et al., 2013), while COSMO uses a generalized Gal-Chen coordinate. WRF's time step is set to 20 and 4 s, while COSMO's time step is set to 90 and 20 s for 12 and 2.2 km simulations, respectively. The simulations were initialized and driven at the lateral boundaries using ERA5 reanalysis (Hersbach et al., 2020) at 12 UTC the day before severe convection was observed. ERA5 surface and pressure levels are used for WRF while COSMO uses three-dimensional ERA5 information. It should be noted that unlike for WRF, soil moisture for COSMO was not initialized from ERA5 reanalysis. Instead, each case simulation was initialized 7 days before the event using the equilibrated monthly mean soil profiles from a 10-year (1999–2008) 12 km COSMO climate simulation (Vergara-Temprado et al., 2020), and let run for 7-day. Then, the model integration started at 12 UTC the day before severe convection was observed using the new soil moisture conditions from the 7 days run. This approach allows for an adjustment

of the top soil layers to the conditions of each event. Physics setups of the models are summarized in Table 2. For the simulation of hail and lightning, HAILCAST (Adams-Selin & Ziegler, 2016) and LPI (Lynn & Yair, 2010; Yair et al., 2010) are used in both models. HAILCAST is a time-dependent hail growth model that provides the forecast of the maximum hailstone diameter at the ground. In our setup, HAILCAST is activated every 5 min on the inner 2.2 km convection-permitting domain if the updraft in a particular grid point exceeds 10 ms^{-1} for more than 15 min. Similarly, we adopt the same formulation of LPI in both WRF and COSMO models. More details on LPI formulation adopted can be found in Brisson et al. (2021). In this study, LPI is computed every 15 and 15 min fields are stored for both models. Additionally, more information on HAILCAST and LPI can be found in Supporting Information S1.

3.2. Evaluation Approach

When evaluating the results of diagnostic tools such as HAILCAST and LPI against observations, it should be considered that their performance relies on the skill of the convection-permitting model to represent the convection properly. For this reason, the results are evaluated in three sequential phases. First, the model's skill to represent the observed precipitation is evaluated. Second, simulated LPI is assessed against LINET lightning data using the minimum coverage neighborhood verification method (Ebert, 2008). Third, HAILCAST results are evaluated against radar estimates on hail occurrence from Switzerland and direct hail measurements from the Croatian hailpad. Moreover, to account for possible time shifts between simulated and observed convection, only daily aggregated fields are evaluated.

Simulated precipitation is assessed against precipitation estimated by IMERG. Given the discrepancy in horizontal grid spacing between IMERG (0.1°) and simulated precipitation (2.2 km), both IMERG and simulated precipitation are interpolated to a common 12 km grid (Table 2). The evaluation is performed by using Taylor diagrams (Taylor, 2001), which compare spatial distribution of simulated and observed fields and summarize the results using statistical metrics.

Evaluation is done by determining standardized deviations, correlation coefficients and root mean square errors between observed and simulated fields.

LPI is assessed against lightning observations from the LINET network. First, to account for the differences in horizontal grid spacing between LINET (3 km) and LPI (2.2 km), simulated fields are interpolated to a common 3 km grid as indicated in Table 2. However, considering that a high-resolution simulation cannot perfectly match the observation in space and/or time, but can still be useful (Ebert, 2008), we are using a minimum coverage neighborhood method. In that approach, a useful forecast is defined as the one where lightning is simulated anywhere in the neighborhood of the point where it is observed. Based on this method, a contingency table is built and a symmetric extremal dependence index (SEDI) (Ferro & Stephenson, 2011) is computed. Additionally,

Table 2
Modeling Setups of COSMO and WRF Models Used in This Study

	COSMO	WRF
Domain	12 km (361×361 grid points) 2.2 km (800×600 grid points)	12 km (361×361 grid points) 2.2 km (801×601 grid points)
Vertical levels	60 Gal-Chen	65 hybrid sigma pressure
Time step	90 s, 20 s	20 s, 4 s
Soil moisture spin up	Yes	No
Cumulus parameterization	12 km Tiedke (Tiedke, 1989) 2.2 km No cumulus scheme	12 km Kain-Frisch (Kain & Kain, 2004) 2.2 km No cumulus scheme
PBL scheme	Prognostic TKE scheme (Raschendorfer, 2001)	MYNN 2.5 (Nakanishi & Niino, 2006)
Microphysics scheme	Single moment Reinhardt and Seifert scheme	WSM6 (Hong & Lim, 2006)
Radiation	Ritter and Geleyn scheme (Ritter & Geleyn, 1992)	RRTM and Dudhia scheme (Mlawer et al., 1997)
Hail	HAILCAST activates every 5 min	HAILCAST activates every 5 min
Lightning	LPI activates every 15 min	LPI activates every 15 min

verification window size as well as threshold for the number of lightning flashes is varied to examine the scale-intensity combination at which high-resolution simulation is useful.

HAILCAST results are assessed against radar products POH and MESHS from Switzerland and hail measurements from the Croatian hailpad network. To evaluate HAILCAST results against radar products, a minimum coverage verification method with varying verification windows sizes is utilized and categorical skill score such as probability of detection (POD), false alarm ratio (FAR) and extremal dependence index (EDI) (Ferro & Stephenson, 2011) are determined. Next, HAILCAST results are assessed against hailpad observation from Croatian hailpad network. To overcome challenges associated with the limited spatial information from hailpad networks and to limit the effect of double penalty that occurs when verifying slightly offset high-resolution forecasts of extremely rare events (Ebert, 2008), an upscaled neighborhood verification method is used (Malečić et al., 2022). This verification methodology is composed of the elements of point to point, upscaling and a minimum coverage verification method (as described by Ebert (2008) and Malečić et al. (2022)). Based on this method, a contingency table is built and categorical skill scores are determined (POD, FAR, EDI).

4. Results and Discussion

4.1. Precipitation

The first step considers the comparison between simulated and observed precipitation. The comparison refers to the period from 00 UTC to 24 UTC on the day when severe convection was observed. When comparing the daily accumulated fields, a generally good agreement between observed and simulated fields is found (Figure 2). Both models reproduce the observed precipitation patterns fairly well, even though there are slight local variations. Moreover, the areas with more intense precipitation correspond well between simulated and observed fields. However, a tendency of both models to produce more peaked and more scattered precipitation objects data is found for all analyzed cases except for 8 July 2017 and 18 June 2013. This tendency could partially be attributed to the differences in horizontal resolution between simulated and observed fields (2.2 and 11 km horizontal grid spacing, respectively). On the other hand, for 18 June 2013 and 8 July 2017, both models produced mostly smaller and less peaked objects than observed. In addition, comparison of COSMO-crCLIM and WRF fields, reveals that WRF tends to produce slightly less peaked precipitation objects than COSMO-crCLIM.

To further expand and complement this analysis, hourly accumulated precipitation averaged over the whole inner domain (Figure 1a) is compared between the observations and the models (Figure 3). To account for discrepancies in the horizontal resolutions between observations and simulated fields, interpolated fields are analyzed, as discussed in Table 3. The comparison reveals that both models reproduce the temporal evolution of precipitation fairly well in all cases, except for 25 June 2017 although some discrepancies exist, depending on the case. For the case of 25 June 2017, both models fail to represent the two local maximums of precipitation observed in the early morning and evening hours. During most cases, both models simulate comparable or slightly larger amounts of precipitation compared to the observations. An underestimation of precipitation is present only for 18 June 2013 and 8 July 2017 cases as already noted above.

The daily accumulated precipitation results are further compared quantitatively using Taylor diagrams (Taylor, 2001). As shown in Figure 4, both models perform similarly, although larger differences in standardized deviations are found for the cases of 18 June 2013 and 8 July 2017. Both models show similar correlation coefficients between simulated and observed fields. Looking at the median performance for all cases together, we can see that both models perform similarly in simulating the observed precipitation with standardized deviations of 1.14 and 1, correlation coefficients of 0.48 and 0.46 and root mean square errors of 1.14 and 1.04 for COSMO-crCLIM and WRF, respectively.

Overall, we can see that both models successfully represent the observed precipitation, and that WRF tends to simulate less precipitation than COSMO-crCLIM.

4.2. Lightning Potential Index Results

The second step of the evaluation considers the assessment of LPI [J/kg] against the observed number of lightning flashes from the LINET network. LPI indicates the potential for lightning activity, and as such, it is not directly connected to the observed number of lightning flashes. To make a direct comparison between LPI and

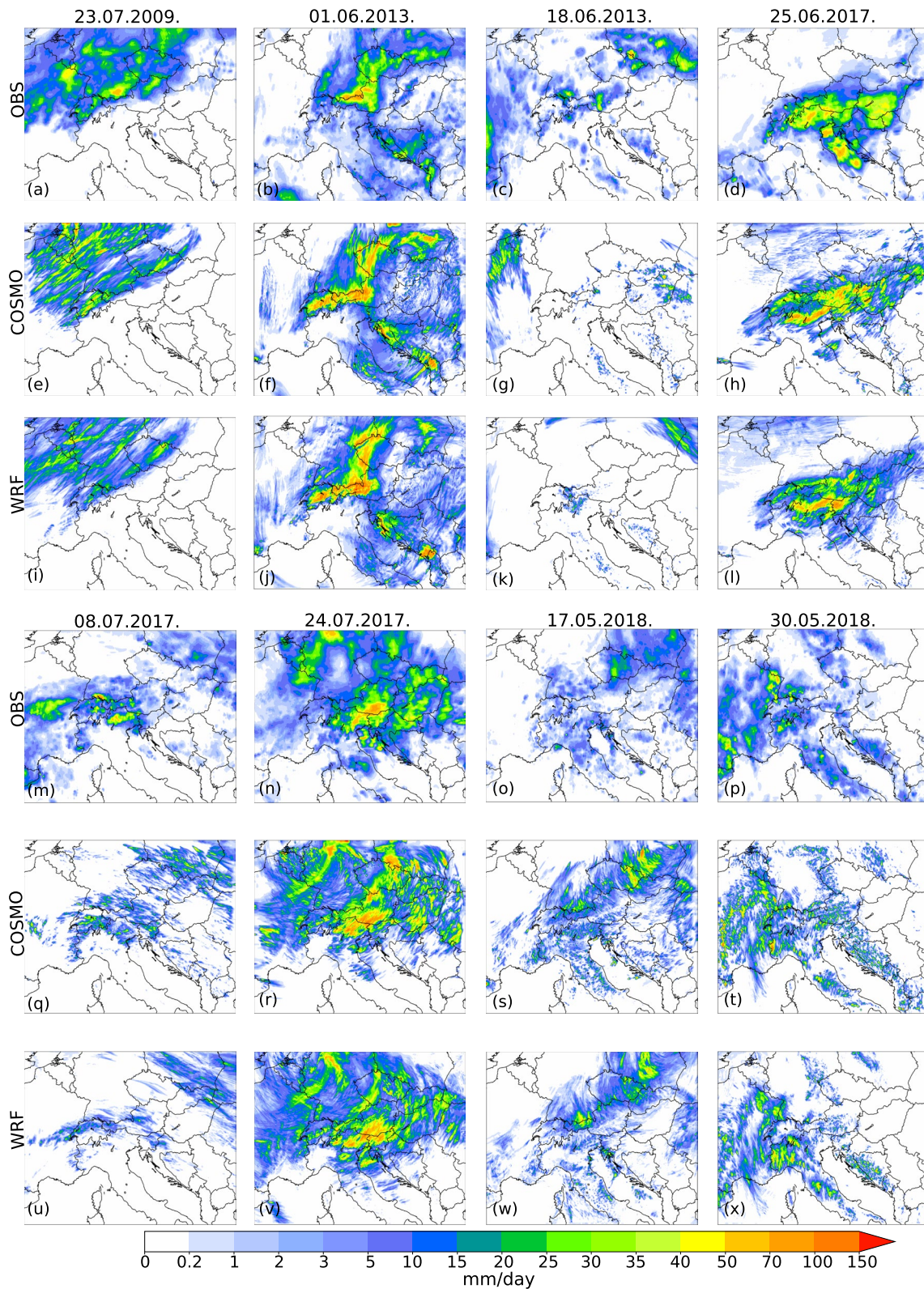


Figure 2. Accumulated precipitation for the period between 00 and 24 UTC on the day severe convection was observed for the eight case studies. The results are presented for (a–d; m–p) IMERG observations, (e–h; q–t) COSMO-crCLIM and (i–l; u–x) WRF simulations.

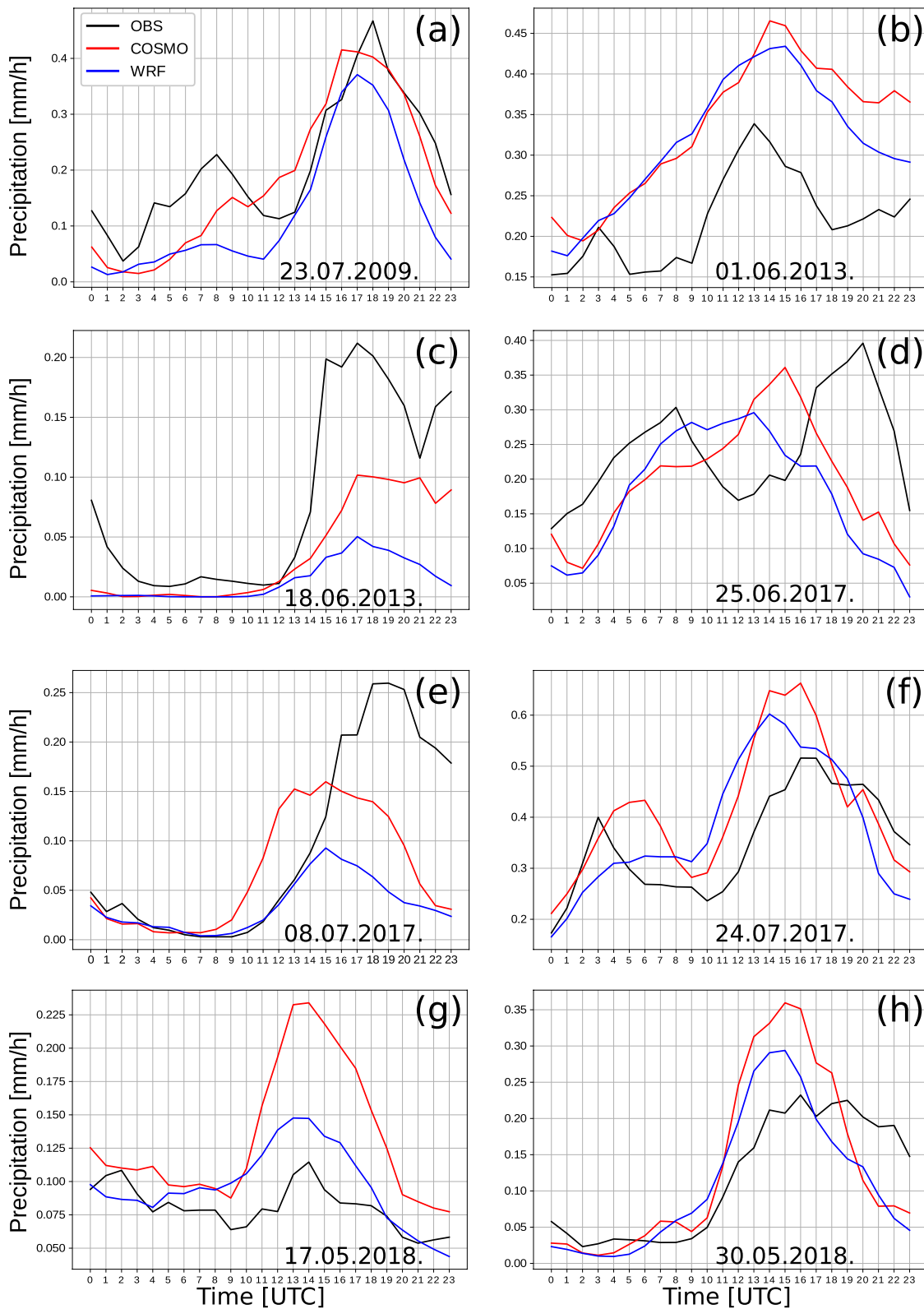


Figure 3. Hourly accumulated precipitation obtained from IMERG (black) observations and simulated by COSMO-crCLIM (red) and WRF (blue) for all eight cases (a–h). The observed and simulated hourly precipitation amounts are interpolated to a 12 km grid and then averaged over the 2.2 km domain.

Table 3
Validation Procedures When Using Fields of Different Spatial Resolutions

Observational data set	Observations horizontal grid spacing [km]	Model horizontal grid spacing [km]	Common grid	Interpolation method
LINET	3	2.2	3 km × 3 km	Distance-weighted
IMERG	11	2.2	12 km × 12 km	Cumulative

Note. The interpolation method as well as the common grids used are indicated.

the observed number of lightning flashes, a conversion of LPI to the number of lightning flashes following Brisson et al. (2021) and Malečić et al. (2022) is done considering LPI and LINET measurements on a common grid (Table 3). Conversion assumes a linear relationship between the LPI and the observed number of lightning flashes as well as the existence of the threshold value of LPI for which a lightning flash is produced, such that:

$$LPI_{adj} = \begin{cases} 0, & LPI \leq t \\ k \cdot LPI + l, & LPI > t \end{cases} \quad (1)$$

where LPI_{adj} [$km^{-2} h^{-1}$] denotes the adjusted LPI, that is, LPI converted to the number of lightning flashes, parameter t denotes the minimum value of LPI for which a lightning flash is produced, k and l represent the parameters of a straight line. The parameters t , k and l are iterated across $[0, 20]$, $[0, 10]$, $[-20, 20]$ intervals, respectively. For every combination of parameters t , k , and l , hourly means of LPI_{adj} are calculated. Then, a distribution function of both simulated and observed hourly means of lightning flashes during all cases is determined. Further, a root mean square error (RMSE) between the two discussed distributions is calculated. The optimal combination of parameters is the one that minimizes the RMSE. Here, a conversion is done by using $t = 0.045$, $k = 3.3$ and $l = 0.1$ for COSMO-crCLIM and $t = 0.65$, $k = 0.65$ and $l = -0.2$ for WRF for all cases. The discrepancy in optimal parameter values between WRF and COSMO highlights the discrepancies between LPI produced by COSMO-crCLIM and WRF. Namely, higher values of t and lower values of k associated with WRF indicate that WRF produces higher LPI, contrary to the results obtained for precipitation where WRF produced slightly lower precipitation amounts compared to COSMO.

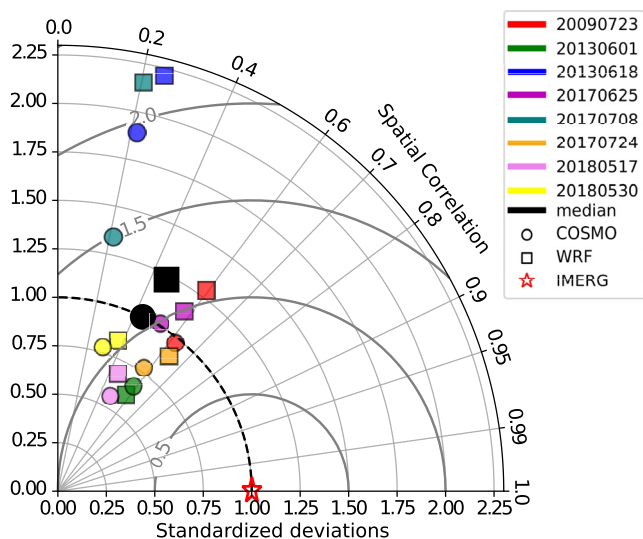


Figure 4. Taylor diagram showing the performance of COSMO-crCLIM (circles) and WRF (squares) when simulating daily accumulated precipitation observed by IMERG (red star). The performance for each case is indicated by colored markers, while the black markers indicate the corresponding median values.

The daily sums of both LPI_{adj} produced by COSMO-crCLIM and WRF and the observed number of lightning flashes for each case analyzed are presented in Figure 5. Overall, it seems that the general spatial pattern of the observed lightning activity is well reproduced by both models although the simulated fields appear to be more scattered than the observed. This could be partially attributed to the fact that LPI is calculated every 15 min, while the LINET network detects lightning flashes continuously. Moreover, considering all cases, it is noted that the conversion of LPI to lightning flashes is better fitted toward less intense lightning activity. This is explained by the fact that the fit is performed on all grid points: as there are more grid points with low flash counts than intense lightning activity, the fit is intrinsically better for lower flash counts. The discrepancy in fit between lower and higher flash counts is more pronounced during the cases with more intense and widespread lightning activity, that is, 25 June 2017 and 24 July 2017. Nonetheless, in general, the spatial distribution of lightning, that is, the distribution of the areas with more and less intense lightning activity, corresponds well between simulated and observed fields, although local discrepancies could be present, depending on the case and model analyzed. Looking at the differences between fields produced by COSMO-crCLIM and WRF, a tendency of COSMO-crCLIM to produce more scattered and less peaked fields can be found.

Furthermore, to quantitatively evaluate the capabilities of COSMO-crCLIM and WRF to simulate the observed lightning activity, a minimum coverage method is utilized. To get more robust results, the evaluation is done

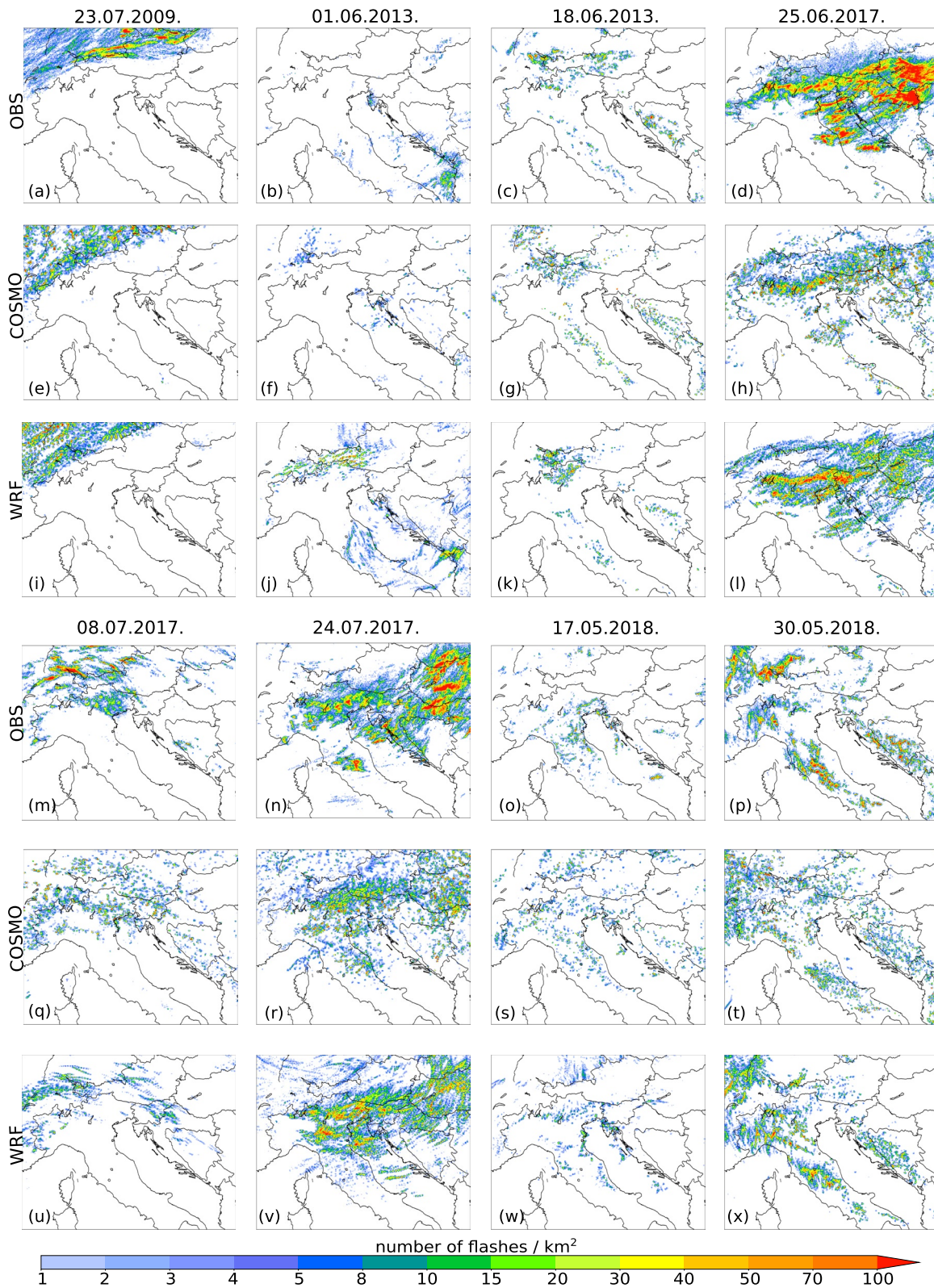


Figure 5. Simulated and observed lightning flash accumulation in the time window from 00 to 24 UTC on the day with severe convection. Columns denote cases, while rows denote measurements from the (a–d; m–p) LINET network, and fields produced by (e–h; q–t) COSMO-crCLIM and (i–l; u–x) WRF models.

by aggregating all analyzed cases together (Figure 6). Both models show similar performance which is better for the lower thresholds of lightning flashes. Moreover, we get good performance (SEDI >0.6) even for more intense thresholds if we consider larger verification window sizes. WRF tends to have higher SEDI values than COSMO-crCLIM toward higher and more localized lightning flashes (bottom right side of diagrams), which confirms the previous findings that COSMO-crCLIM tends to produce more scattered lightning activity.

4.3. HAILCAST Results

HAILCAST results are assessed against remote-sensing and ground observations for a period from 00 UTC to 24 UTC on the day severe convection was observed. First, we perform a qualitative comparison between hail swaths produced by the two models. Figure 7 suggests that both models produce generally similar hail swaths over the same area, although some local discrepancies between simulated hail swaths exist. Despite the overall similarity of the results, a tendency of COSMO-crCLIM to produce more hail in all analyzed cases is apparent. Both models correctly reproduce heavy precipitation without hail over the Alps for 1 June 2013, which suggests that both models are able to distinguish intense precipitation events from hail events. However, it should be noted that both models still produce hail over only a few grid points over the Alps.

Figure 8 shows the simulated and observed hail swaths over the Alpine region. Since POH indicates the probability of hail, and HAILCAST the simulated maximum hailstone diameter, only the spatial distribution of hail as observed by POH and simulated by HAILCAST is compared. It is clear that both models can produce hail swaths comparable to those observed, both in the context of the area affected by hail and the shapes of the observed hail swaths. Notably there is not an exact match between simulated and observed fields, as, some deviations are present. For most cases, WRF produces smaller hail swaths than COSMO-crCLIM, while on the other hand, WRF simulates more grid points having maximum hailstone diameters greater than 35 mm.

Next, we assess simulated fields against another source of hail observations—hailpad observations from the Croatian hailpad network. Out of eight cases with severe convection over the Alpine-Adriatic region, hailpads in Croatia recorded hail on only three of those days (25 June 2017, 24 July 2017, 17 May 2018). For these days, simulated hail swaths with indicated impacted hailpads are presented in Figure 9. There is a generally good agreement between observed and simulated hail produced by both models. Most of impacted hailpads are within the area of simulated hail. However, both models exhibit a certain number of false alarms, that is, hail is not observed, but the model simulates hail. Notably, some of these false alarms could be attributed to the limited spatial information on hail occurrence provided by the hailpad network. Unlike radars, the hailpad network provides information on hail occurrence only at

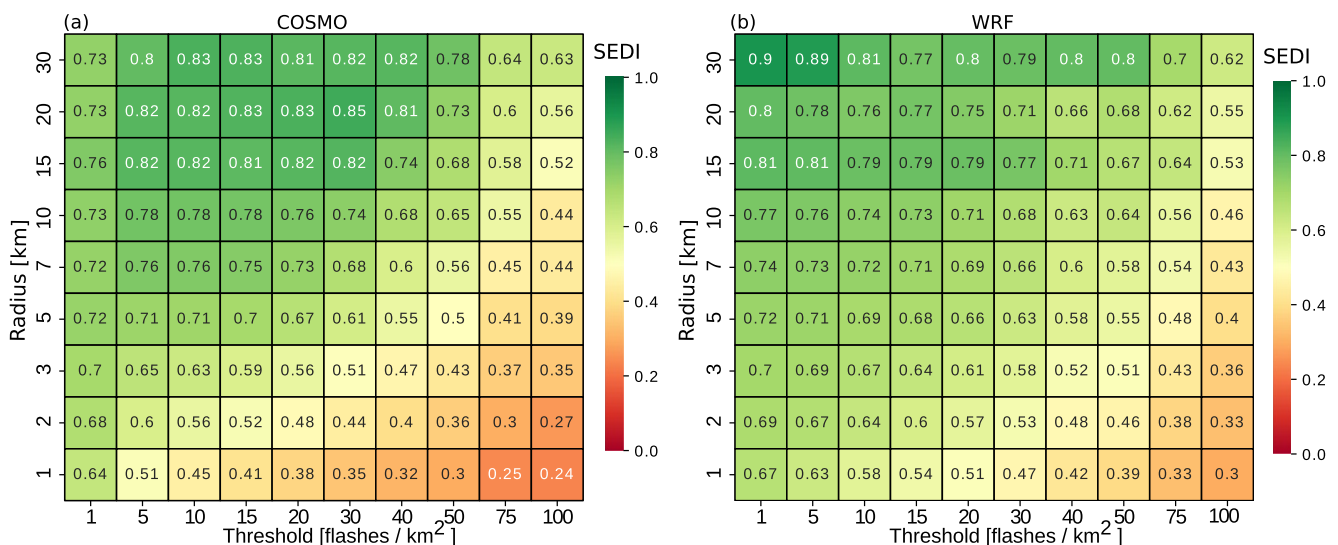


Figure 6. Performance of (a) COSMO-crCLIM and (b) WRF in simulating the observed lightning flashes. Performance depending on the threshold for the number of lightning flashes and verification window sizes (radius) is indicated in terms of SEDI skill score (shading). The higher/lower SEDI score means better/worse performance of the model, as reflected by the green/red colors.

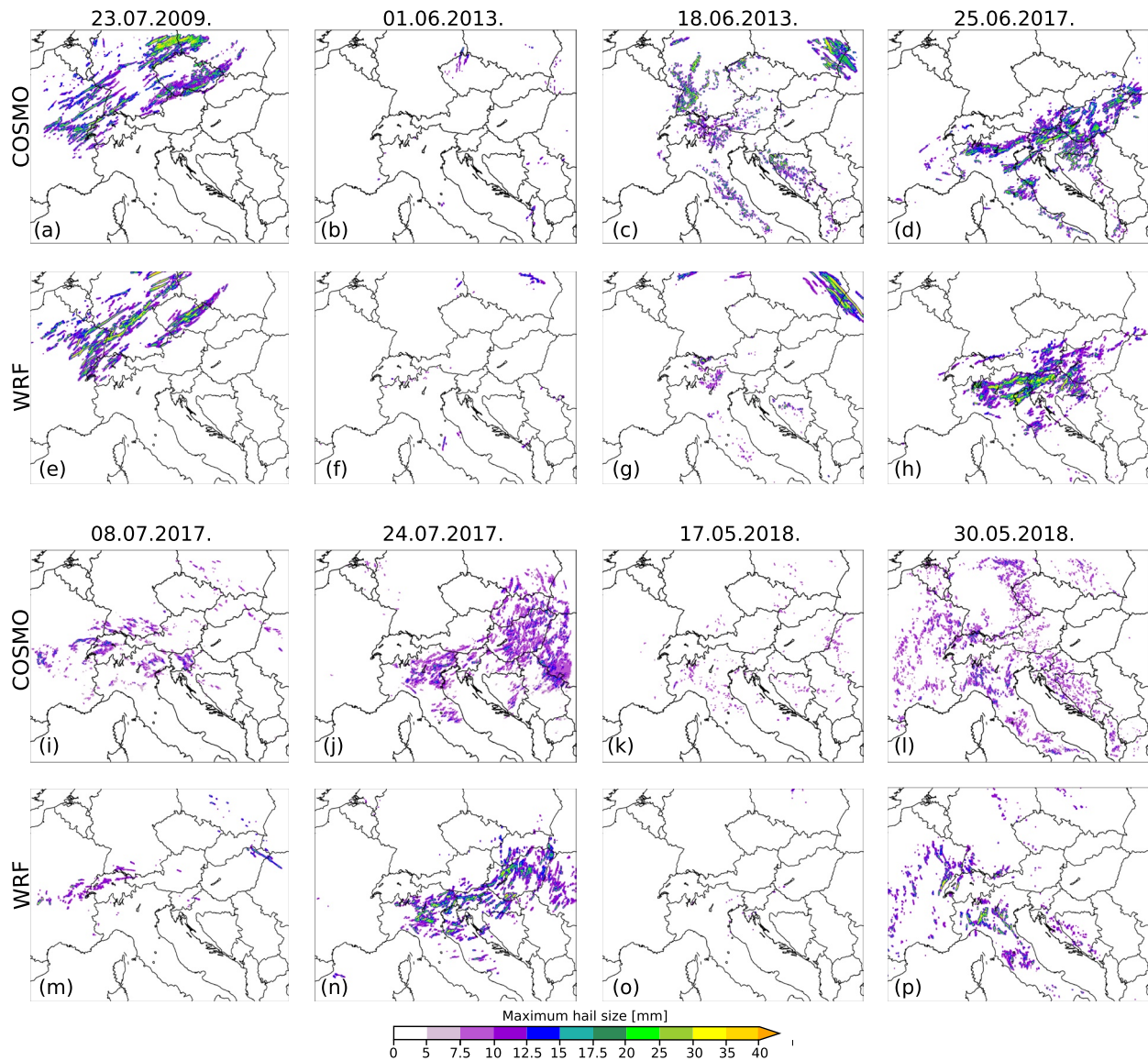


Figure 7. Maximum hailstone diameters in the time window from 00 UTC to 24 UTC on the day with severe convection simulated by COSMO-crCLIM (a–d); (i–l), and WRF (e–h); (m–p).

the exact position where the hailpad is installed. In theory, hail could easily occur anywhere between the two hailpads and be left unrecorded. Nonetheless, the greatest number of false alarms is present for the 24 July 2017 case with WRF producing more false alarms than COSMO-crCLIM. Surprisingly, both models successfully reproduce even a highly localized hailstorm occurring on 17 May 2018 with a flat surface pressure distribution over the north-eastern Adriatic, although it should be noted that, unlike WRF, COSMO-crCLIM produces a few spurious false signals in the continental part of Croatia. Moreover, two of the analyzed cases, namely 25 June 2017 and 24 July 2017, previously analyzed in Malečić et al. (2022), but simulated with different modeling settings (i.e., different domains, horizontal resolutions, input data or HAILCAST activation time), show similar hail swaths in both studies produced by WRF. Notably, in the future, other indices commonly used for estimating hail size such as hail size index, large hail parameter, significant hail parameter could also be investigated and added to the analysis (Czernecki et al., 2019).

The fields presented in Figure 8 are assessed against POH $\geq 80\%$ signals, as the region corresponding to POH $> 80\%$ is highly probable to have hail on the ground (Nisi et al., 2016). Obtained performance diagrams for all 8 cases together presented in Figures 10a and 10b reveal that COSMO-crCLIM performs better in terms of POD and EDI skill scores for all considered verification window sizes. On the other hand, WRF performs better in

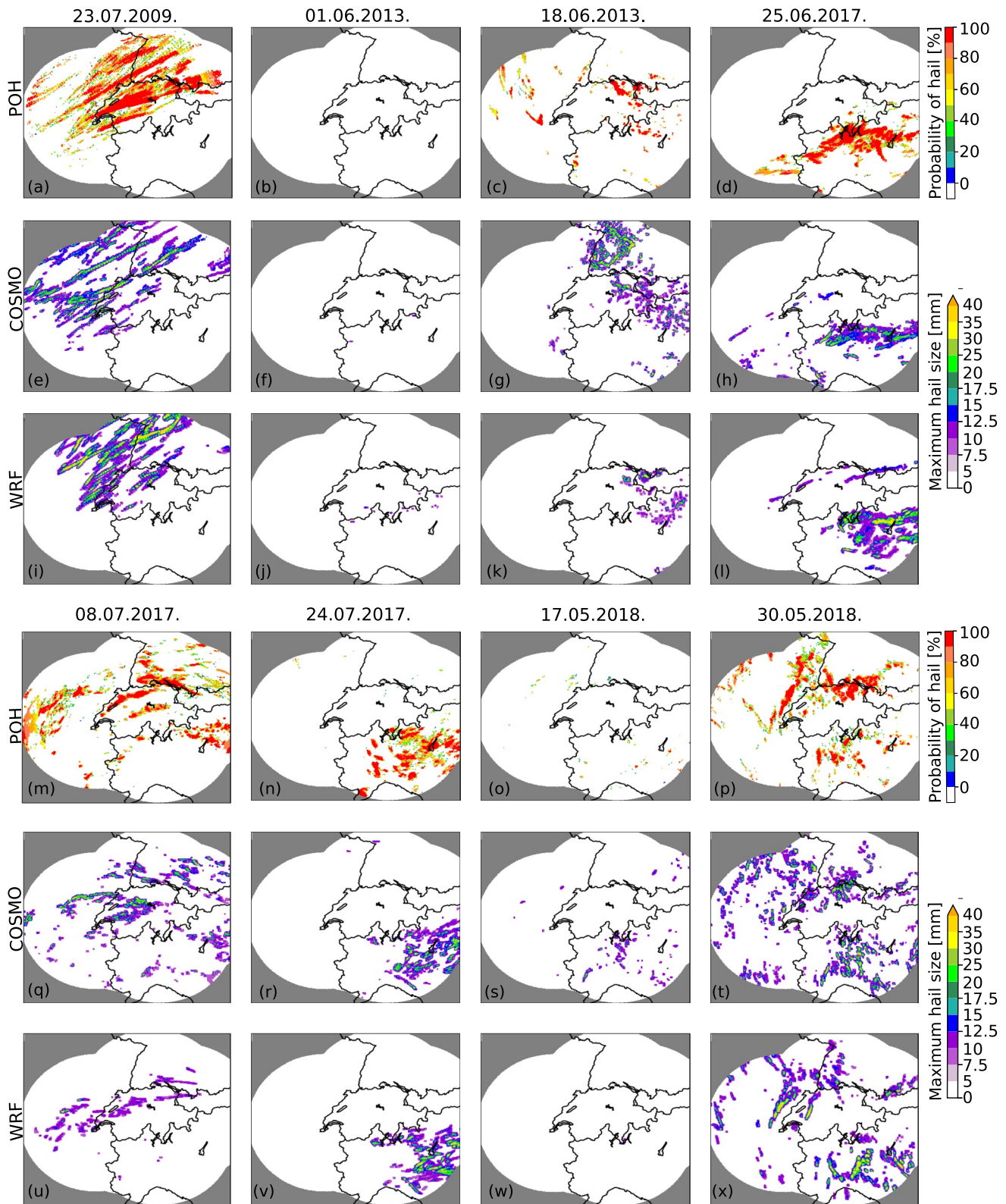


Figure 8. Daily maximums of the hailstone diameter simulated by (e–h); (q–t) COSMO-crCLIM and (i–l); (u–x) WRF and daily maximums of (a–d); (m–p) POH radar product.

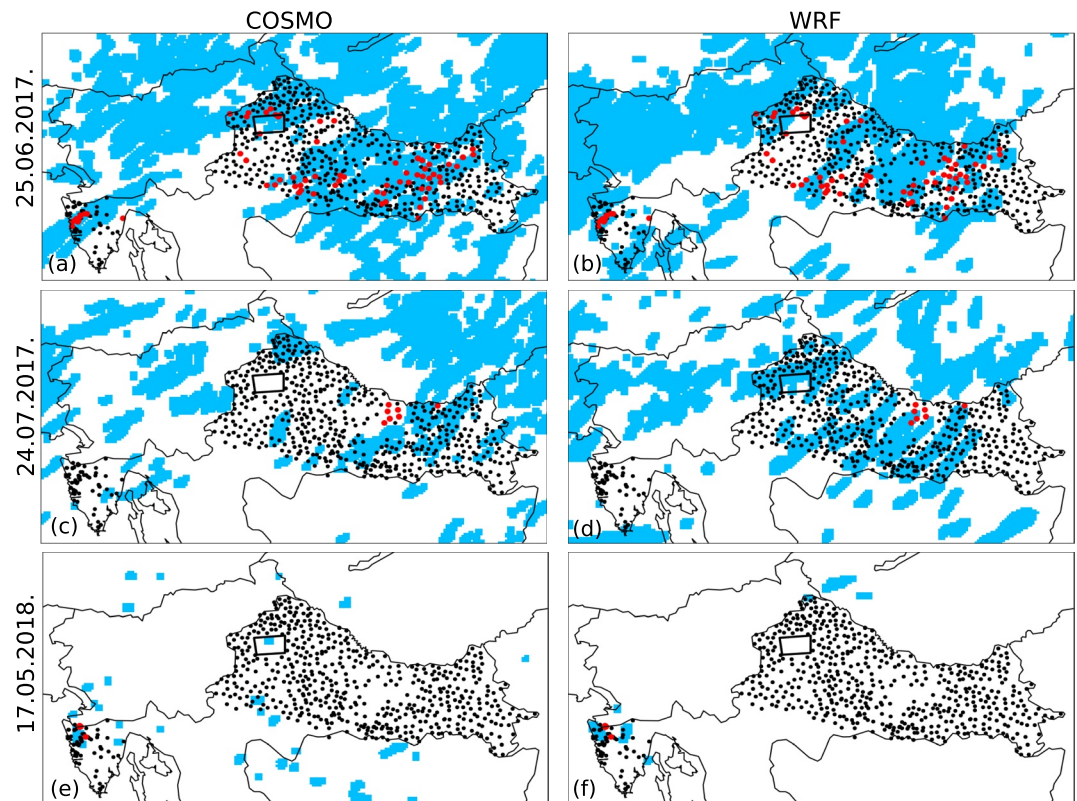


Figure 9. Simulated and recorded hail during the three cases with hail in Croatia. The shaded blue area represents simulated hail swaths (maximum hailstone diameter larger or equal to 5 mm) from 00 to 24 UTC on the day hail was observed. The position of hailpads is indicated with black dots. Impacted hailpads are marked with red circles. The position of a densely populated hailpad polygon is marked with a black rectangle and the stations within the polygon are colored only if the hail was observed at that specific station. Fields produced by (a, c, e) COSMO-crCLIM and (b, d, f) WRF are presented.

terms of FAR for all verification window sizes except the one corresponding to 30 grid points. These findings could be attributed to the fact that COSMO-crCLIM produces more hail compared to WRF, which leads to higher POD and FAR values. According to the insights obtained in Figures 8, 10a and 10b, COSMO-crCLIM tends to produce hail swaths more similar to those observed than WRF over the Alpine region.

Next, simulated fields are evaluated against observations from the hailpad network in Croatia. The obtained performance diagrams for all three cases together (Figures 10c and 10d) show similar performance between the models. High POD values for larger verification window sizes indicate that models simulated hail where it was observed. However, unlike the results connected with radars (Figures 10a and 10b), FAR values associated with the hailpad network are much higher. That could be connected to the potential tendency of the model to overestimate the area affected by hail, if not also to the lack of spatially continuous information on hail occurrence in Croatia. Notably, there is a great contribution to the FAR values from the case on 24 July 2017 where both models produce a lot of false alarms. Interestingly, the same case, 24 July 2017, was also poorly represented in Malečić et al. (2022) using different modeling setups with a lot of false alarms indicating a low predictability of the atmospheric conditions leading to the initiation and evolution of the observed convection.

Hailpad networks, besides delivering information on hail occurrence, also provide information on hailstone sizes on the ground. Based on this information, a comparison of simulated and observed maximum hailstone diameters is performed. To account for possible spatial shifts between observed and simulated fields, a neighborhood inside a radius of 5 grid points (roughly corresponding to 12 km) of each impacted hailpad is scanned. The maximum simulated hailstone diameter inside this area is compared to the observed maximum hailstone diameter (Figure 11a). Both models underestimate the occurrence of smaller hailstones (diameters of 5–10 mm and 10–20 mm) and overestimate the occurrence of larger hailstones (diameters larger than 20 mm). However, when analyzing such results, one should proceed with caution, as it has been known from previous studies that hailpads

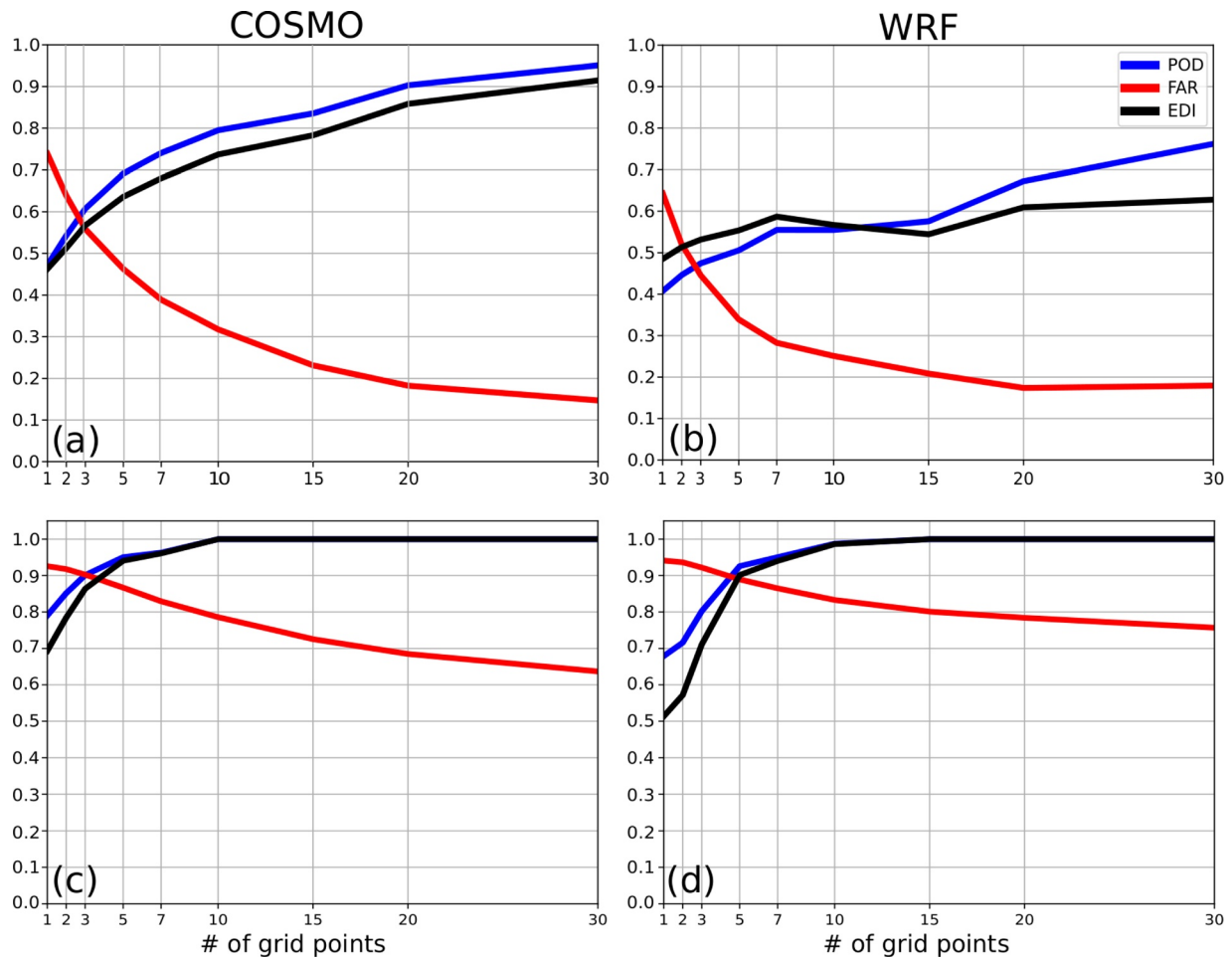


Figure 10. Performance of (a) COSMO-crCLIM and (b) WRF to simulate hail swaths as observed by the probability of hail (POH) radar product, and performance of (c) COSMO-crCLIM and (d) WRF in simulating hail as observed by the Croatian hailpad network in terms of probability of detection (POD, blue), false-alarm rate (FAR, red) and extremal dependence index (EDI, black) skill scores. Performance depending on the verification window size is presented.

are unlikely to record the largest hailstones given that they cover only 0.25 m² (Smith & Waldvogel, 1989). Indeed, to obtain a more realistic comparison between simulated and observed maximum hailstone diameter, it would be better to use the information on hailstone size observed by an observer—data that was not available for this study. Nonetheless, some tendencies could be extrapolated from the present comparison. Namely, COSMO-crCLIM mostly simulates hailstones in the 20–30 mm category, while WRF mostly simulates hailstones in the 30–50 mm category. Additionally, WRF was able to reproduce an observed hailstone larger than 50 mm. Those differences between the two models are further confirmed if we compare the distribution of maximum hailstone sizes over the whole domain and all cases (Figure 11b). Here, it is clear that COSMO-crCLIM produces more hailstones in the 5–10 mm category than WRF, while WRF tends to produce more larger hailstones.

4.4. Differences Between Models and Model Internal Variability

The analysis reveals that WRF tends to produce less precipitation, smaller hail swaths but higher values of LPI and more large hailstones compared to COSMO-crCLIM. Here, we study the potential origins of these differences, and consider the role of model internal variability in our results. For this reason, we form an ensemble of simulations with different initialization times for one of the cases with widespread hail and lightning across the Alpine-Adriatic region, namely the 30 May 2018. Both models were initialized at 06, 12 and 18 UTC the day before hail was observed (29 May 2018). Additionally, we utilize a simulation of the newest version of COSMO,

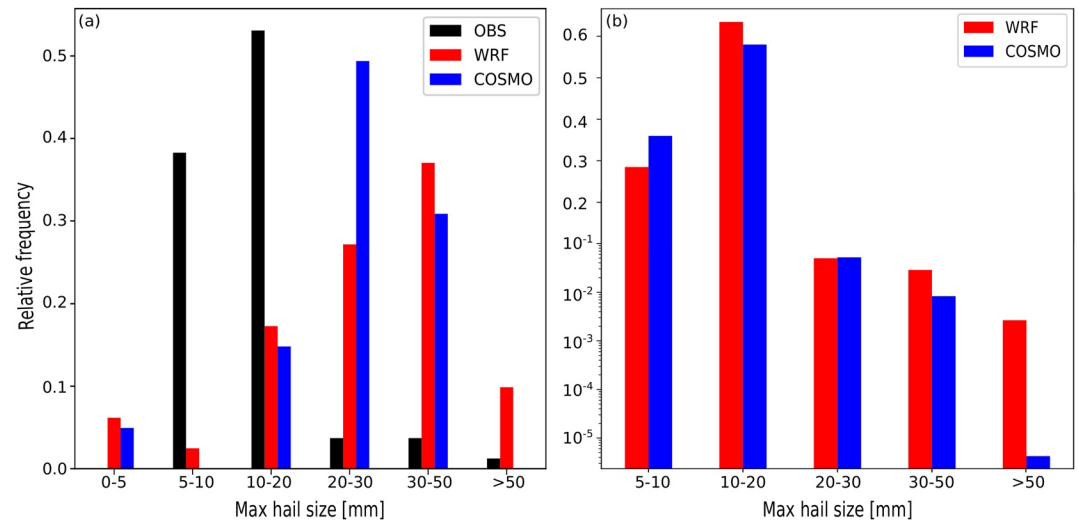


Figure 11. (a) Relative frequency of maximum recorded hailstone size from hailpads (black) and simulated maximum hailstone size by COSMO-crCLIM (blue) and WRF (red), and (b) the relative frequency of simulated maximum hailstone sizes over the whole domain for COSMO-crCLIM (blue) and WRF (red). Histograms are normalized by dividing the count of hailstone sizes in each category with the total observed number of hailstones. To better depict differences between models and runs, the y-axis in (b) is partly linear and partly logarithmic.

namely COSMO 6.0, to further increase the ensemble size and to increase the robustness of our conclusions. The simulation using COSMO 6.0 is initialized at 12 UTC the day before hail was observed.

First, we analyze simulated daily precipitation fields between ensemble members (Figure 12 and see that all ensemble members produce precipitation patterns similar to the observed. Moreover, there is a greater difference in the fields produced by COSMO and WRF than between the members of the same model. This finding suggests that the differences in results are rather linked to systematic differences between models than to the model's internal variability. However, it should be noted that differences between model members exist. Both versions of COSMO produce comparable fields, although local differences are present that may be relevant for forecasting applications. For instance, the observed heavy precipitation along the French-German border is largely or completely missed in two of the COSMO ensemble members but present in the member initialized at 06 UTC. This highlights the need for using ensemble techniques in numerical weather prediction (NWP) applications (Klasa et al., 2018).

Similarly, daily maximums of LPI produced by each of the ensemble members are compared against daily sums of the number of lightning flashes from the LINET network (Figure 13). Here we use the raw LPI instead of the adjusted LPI because we want to avoid filtering the signals to have a direct comparison. It is clear that both models reproduced the area affected by lightning fairly well, although WRF produces higher values of LPI. This finding is consistent with the above results, for which we applied a higher threshold for WRF to convert LPI to the observed number of lightning flashes. Although there are differences in LPI between the model members, there are larger differences in LPI produced by the two different models. COSMO 6.0 produced LPI in agreement with COSMO-crCLIM, although with slightly higher values.

By comparing daily maximums of the hailstone diameters produced by ensemble members for both spatial (Figure 14) and cumulative distribution (Figure 15), similar conclusions are found. Figure 14 shows that the simulated fields are overall similar, although WRF produces less hail compared to COSMO regardless of the initialization time. Hail produced by the same model but different initialization times (06, 12 and 18 UTC) and different model versions (COSMO-crCLIM and COSMO 6.0) is more similar than hail produced by different modeling systems (WRF vs. COSMO). When comparing simulated maximum hailstone diameters (Figure 15), we notice that, for hailstones smaller than 30 mm, the differences between COSMO and WRF are within each model's internal variability. However, for hailstones larger than 30 mm, not only the differences between models

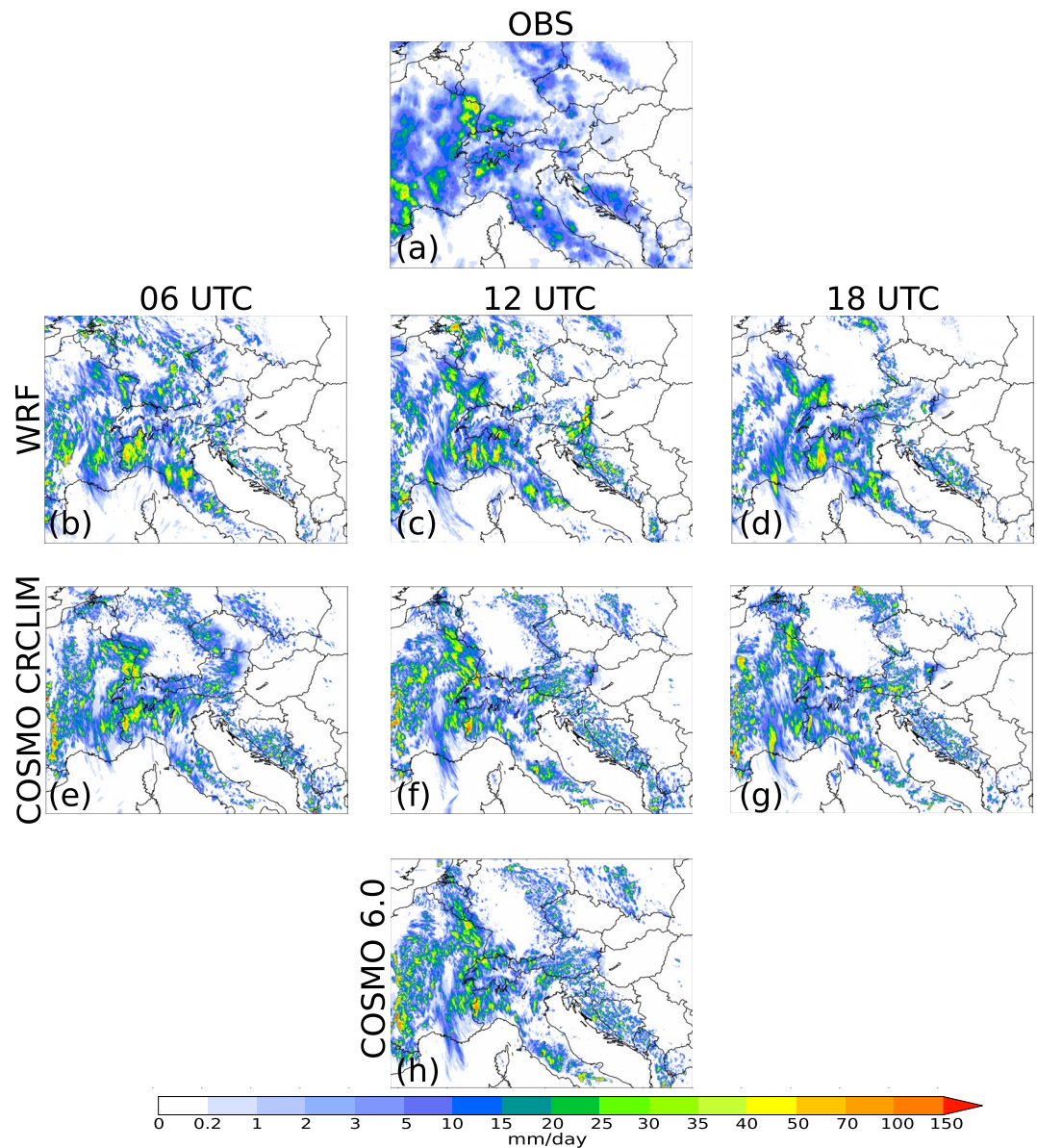


Figure 12. Accumulated precipitation for the period between 00 and 24 UTC on 30 May 2018. From top to bottom rows are (a) IMERG observation and simulated fields using (b–d) WRF, (e–g) COSMO-crCLIM, (h) COSMO 6.0. The columns from left to right represent the simulations initialized at 06, 12 and 18 UTC on the day before the event, respectively.

become larger than model internal variability, but also it is clear that, out of all ensemble members, only WRF produced hailstones larger than 50 mm.

It should be noted that these findings are valid for one case only, and since the magnitude of the internal variability depends on the synoptic situation, model configuration, region and season (Lavin-Gullon et al., 2021), more cases should be analyzed to get more robust conclusions.

Further, considering the importance of the updrafts, as well as solid and liquid hydrometeors in the LPI and HAILCAST formulations, vertical profiles of these variables are compared among the models. Figure 16 presents vertical profiles averaged over time and grid points that have LPI greater than 0 during the 30 May 2018 case. The models produced different distributions of solid and liquid hydrometeors inside thunderclouds. Namely, WRF produces higher cloud water mixing ratios compared to both versions of COSMO and higher rain water mixing ratios compared to COSMO-crCLIM, but lower rain water mixing ratios compared to COSMO 6.0. Similarly,

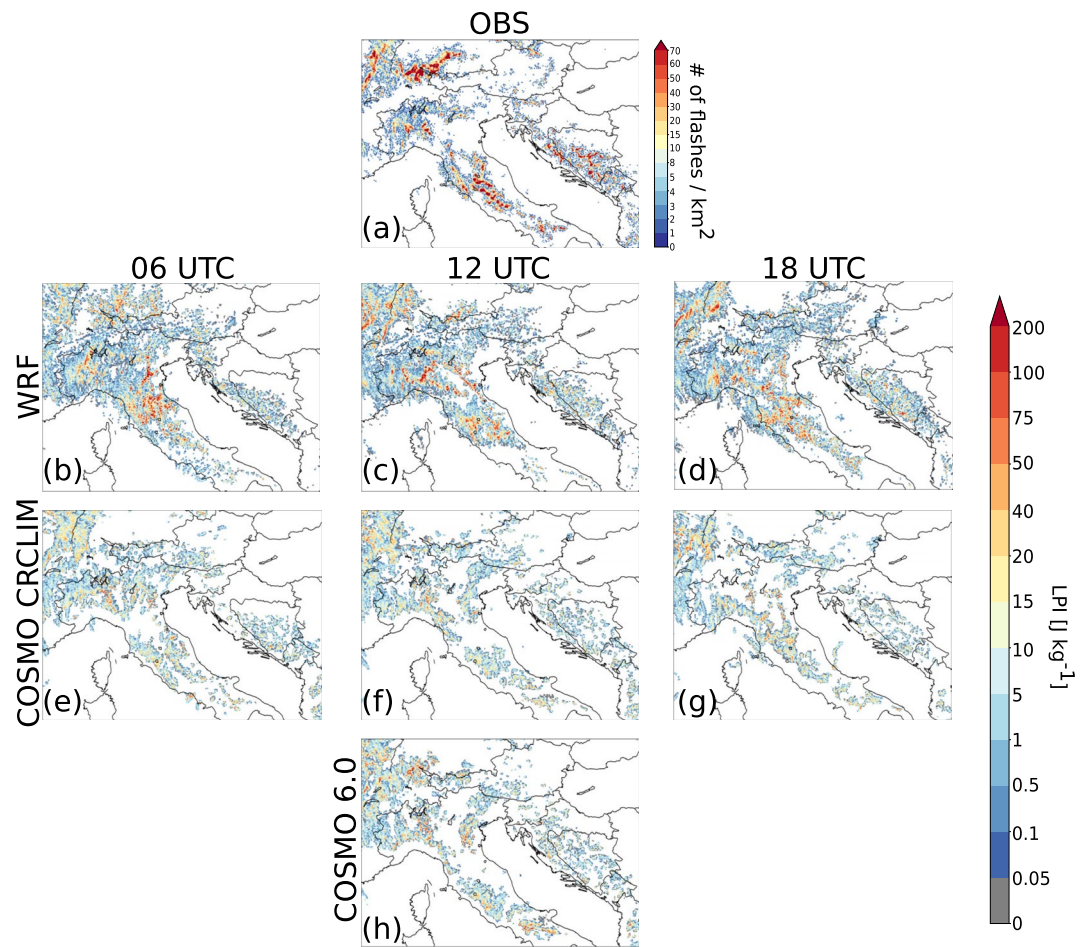


Figure 13. (a) Daily sum of the observed lightning flashes by the LINET network for the period between 00 and 24 UTC on 30 May 2018. Daily maximum of LPI produced by (b–d) WRF, (e–g) COSMO-crCLIM, and (h) COSMO 6.0. The columns represent simulations initialized at with 06, 12 and 18 UTC on the day before the event.

both versions of COSMO produce higher ice and graupel water mixing ratios, but lower snow water mixing ratios. Since in the LPI formulation, the ratio between solid and liquid hydrometeors inside a thundercloud is more important than their exact values, total liquid water and ice fractional liquid ratio terms from the LPI formulation (Q_L and Q_I terms from Equations S2.2 and S2.3 in Supporting Information S1) are computed alongside a dimensionless parameter ϵ representing the scaling factor for the updraft in the LPI formulation (Equation S2.1 in Supporting Information S1). ϵ obtains maximum values when total liquid water and ice fractional mixing ratios are equal (Equation S2.2 in Supporting Information S1). Surprisingly, analysis of ϵ shows no apparent discrepancies between the models even though there are some differences in Q_L and Q_I parameters. However, there is a difference in the simulated updrafts, that is, both COSMO versions simulate, on average, weaker and higher updraft cores compared to WRF. WRF simulates stronger updrafts with the updraft core exactly at the position of the maximum value of ϵ , coinciding with the region with nearly equal amounts of solid and liquid hydrometeors. Since the presence of both solid and liquid hydrometeors is important for lightning and hail growth processes, it is not surprising that WRF simulates higher LPI and more large hailstones compared to COSMO. On the other hand, the updraft core in both versions of COSMO is in the region with much more solid than liquid hydrometeors which is not as favorable for lightning or hail growth processes. This could be the reason why COSMO simulates lower LPI values and higher amounts of smaller hailstones. COSMO 6.0 simulates stronger updraft cores compared to COSMO-crCLIM which could explain why COSMO 6.0 produces higher LPI values than COSMO-crCLIM (Figure 13) and larger hailstones compared to COSMO-crCLIM (Figure 15a).

Several studies reported a sensitivity of hail and lightning-related variables such as updrafts and graupel mixing ratios on the choice of microphysics (Lagasio et al., 2017; Manzato et al., 2020; Raupach et al., 2021;

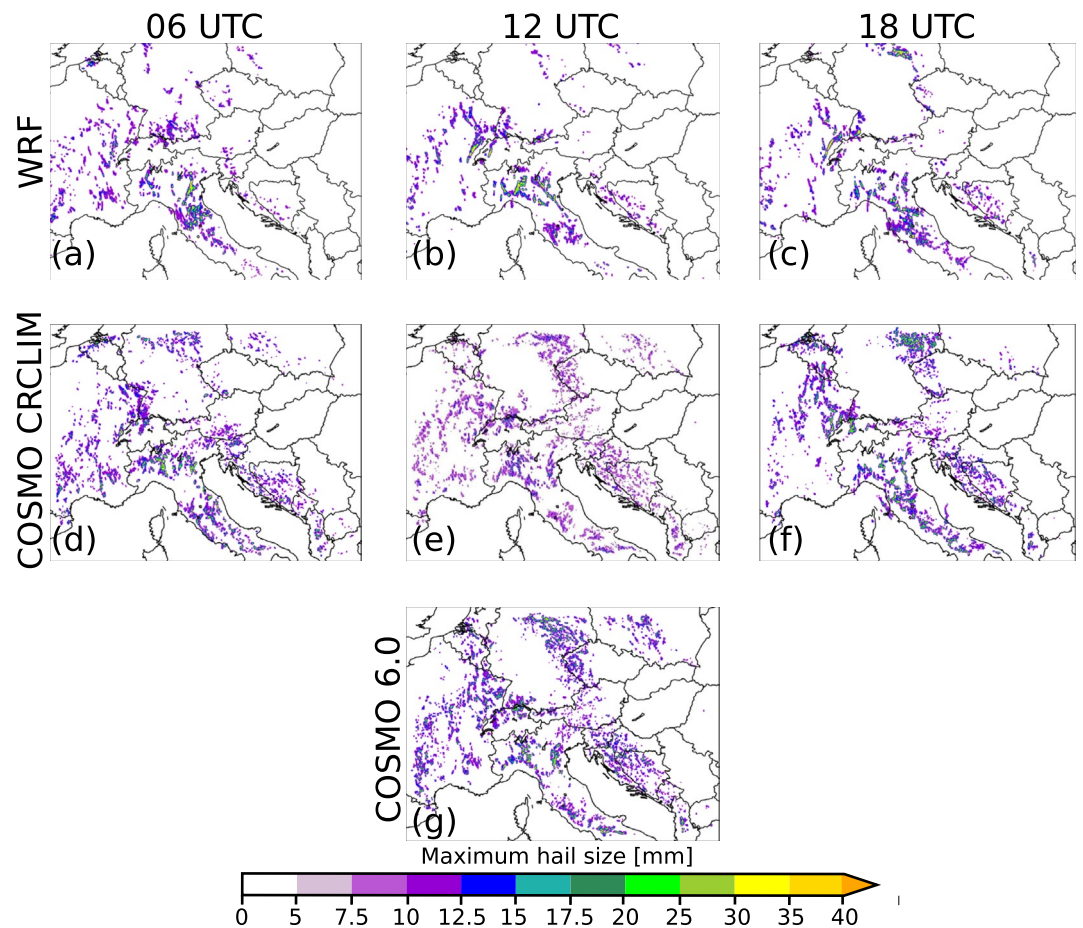


Figure 14. Daily maximum of hailstone size for the period between 00 and 24 UTC on 30 May 2018 simulated by (a–c) WRF, (d–f) COSMO-crCLIM, and (g) COSMO 6.0. The columns represent the simulations initialized at 06, 12 and 18 UTC on the day before the event.

Sokol & Minářová, 2020; Trefalt et al., 2018), a combination of microphysics and planetary boundary layer parameterization scheme (Malečić et al., 2022), and large-scale forcing and initialization time (Manzato et al., 2020). Thus, different models with different configurations can produce large variability for different cases.

Likewise, differences in updrafts strength and structure strongly depend upon the dynamical core of the models. Such differences can objectively be assessed using kinetic energy spectra (Skamarock, 2004). While both models considered here have similar dynamical cores using the split-explicit approach, there are significant differences in terms of advection schemes. The role of model formulation for heavy summer convection over Europe has recently been investigated in an intercomparison of the COSMO and the ECMWF-IFS models (Zeman et al., 2021). Results revealed a strong sensitivity with respect to the dynamical core (split-explicit vs. spectral) but also with respect to time-step size as well as (explicit or implicit) numerical diffusion.

5. Conclusions

Hail and lightning, which are damaging and relatively frequent phenomena over the Alpine-Adriatic region, still remain difficult to model. Thus, this study employed two km-scale models, namely COSMO and WRF, with hail (HAILCAST) and lightning (LPI) diagnostic tools to simulate eight severe convective events occurring over the Alpine-Adriatic region. The main aim was to analyze the robustness of HAILCAST and LPI results produced by

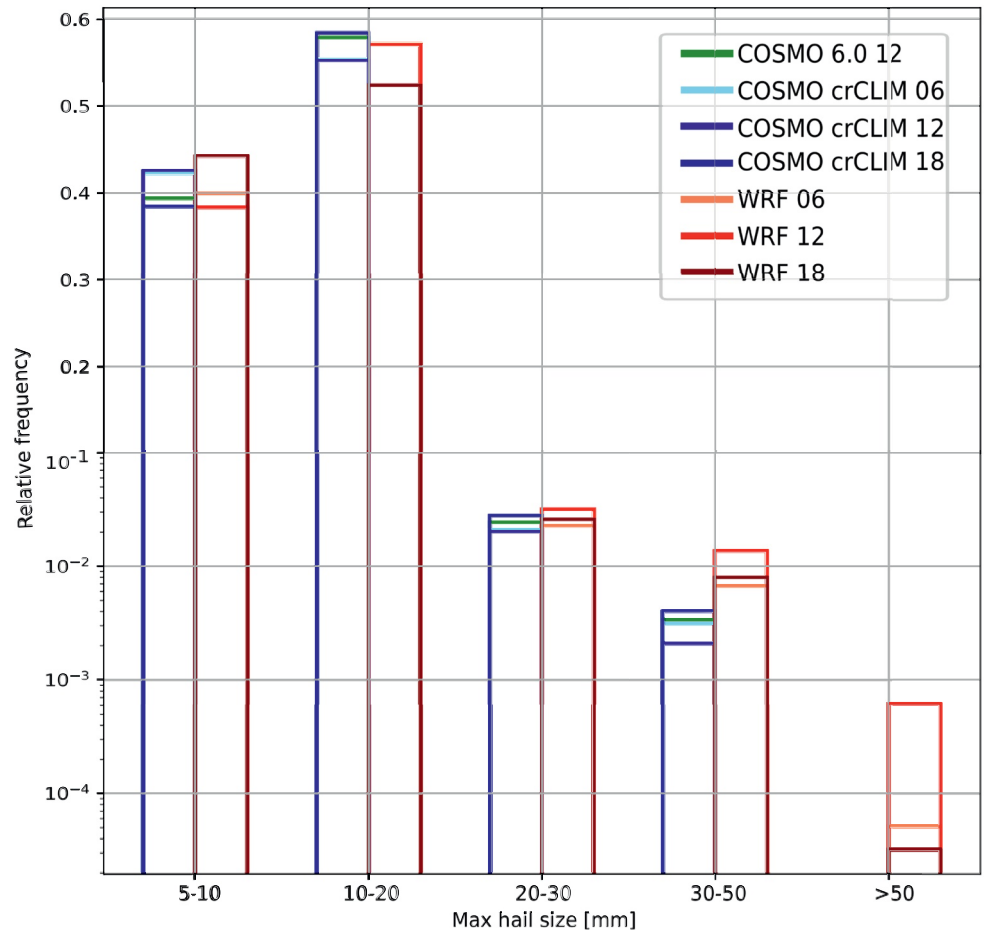


Figure 15. Relative frequency of the simulated maximum hailstone diameters over the whole domain for COSMO-crCLIM initialized at 06, 12 and 18 UTC (shades of blue), WRF initialized at 06, 12 and 18 UTC (shades of red) and COSMO 6.0 initialized at 12 UTC (green). The histograms are normalized by dividing the count of hailstone sizes in each category with the total number of grid points where hail occurs. To better depict differences between models and members, the y-axis is partly linear and partly logarithmic.

the two different modeling systems, to explore their differences and to systematically and quantitatively evaluate the performance of each model. The main conclusions from this analysis can be summarized as follows.

- Both models reproduced the observed spatiotemporal precipitation characteristics, with WRF producing slightly lower amounts.
- Both models showed good performance in reproducing the observed lightning activity despite WRF's tendency to simulate higher LPI values.
- Simulated hail swaths are overall similar, with COSMO tendency to produce more hail. Both models showed a good performance in reproducing hail observed by radar estimates over Switzerland and in-situ measurements over Croatia, although COSMO performed slightly better than WRF. Both models, on average, overestimated observed maximum hailstone diameters, with WRF tendency to produce larger hailstones
- Differences between the models are present regardless of their initialization time and can be linked to different distributions of updrafts and hydrometeors inside thunderclouds.

In conclusion, we show that atmospheric conditions leading to hailstorm formation and evolution are well simulated using state-of-the-art km-scale modeling systems. Moreover, HAILCAST and LPI have great potential for real-time forecasting and climatological assessment of hail and lightning in current and future climates. However, the variability of the results depending on the modeling system used encourages the use of a multi-model and/

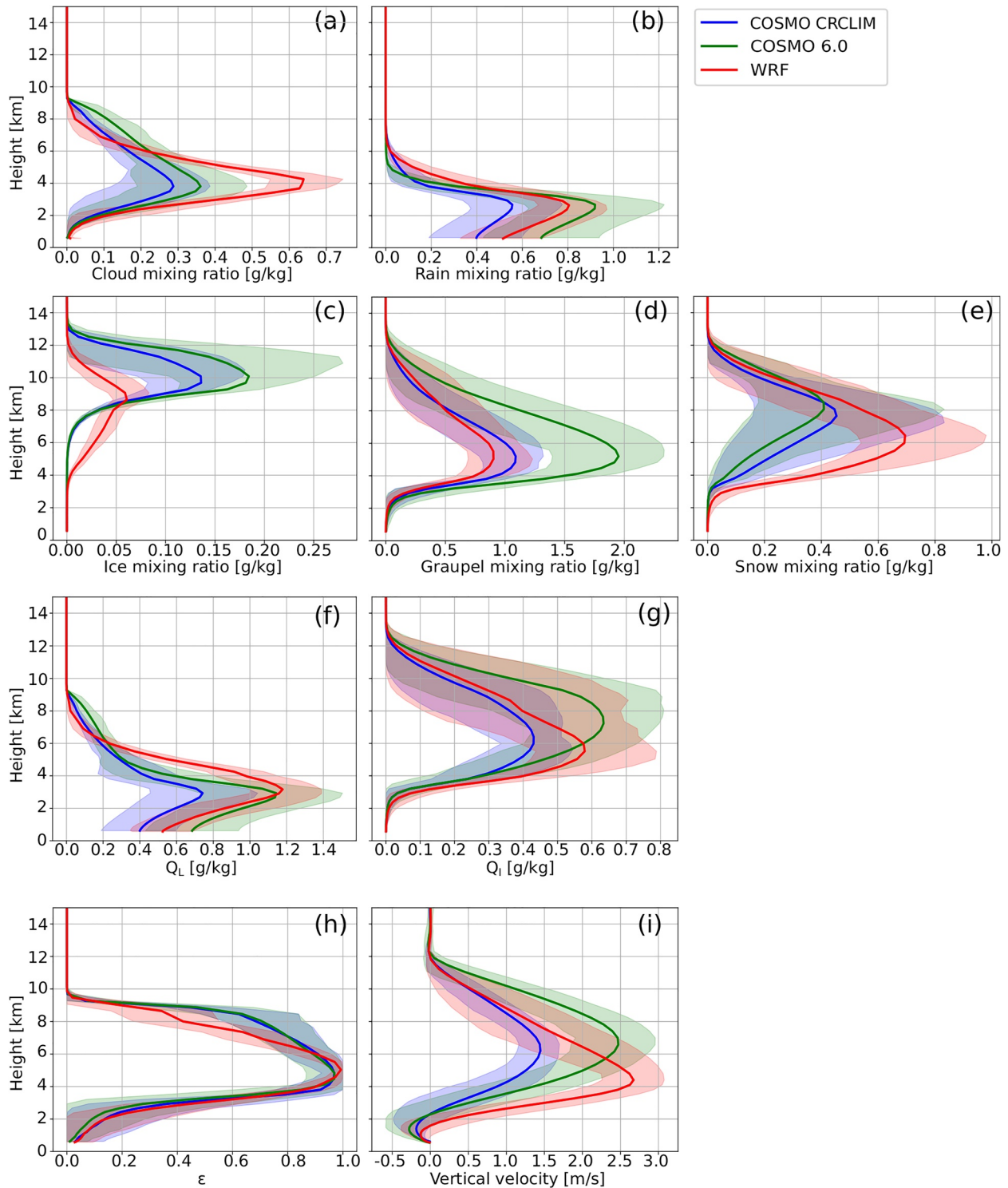


Figure 16. Vertical profiles of (a) cloud, and (b) rain mixing ratio; (c) ice, (d) graupel, (e) snow, (f) total liquid water, and (g) ice fractional mixing ratio; (h) updraft scaling parameter; and (i) vertical velocity as simulated by COSMO-crCLIM (blue), COSMO 6.0 (green) and WRF (red) models. The lines indicate the mean values across all grid points with LPI > 0, while the shading indicates the range between 5th and 95th percentile.

or multi-physics ensemble when modeling such events. Despite the promising results, it should be noted that this study is based on a small number of cases. To get statistically more robust conclusions a larger number of hailstorms needs to be analyzed. Moreover, this study would highly benefit from employing other data sources of hail observations covering the whole Alpine-Adriatic region. Nonetheless, given all limitations, this study represents the first attempt to systematically analyze and evaluate the performance of two intrinsically different km-scale modeling systems to reproduce the main characteristics of multiple hailstorms occurring over the Alpine-Adriatic region.

Data Availability Statement

Data for this research were obtained from three sources. Lightning data were obtained from the Lightning Detection Network in Europe (LINET) <https://www.nowcast.de/en/solutions/linet-data> (Betz et al., 2009). ERA 5 reanalysis fields used as initial and boundary conditions can be obtained through the following link (<https://cds.climate.copernicus.eu#!/home>) while the IMERG dataset can be obtained through (<https://gpm.nasa.gov/data/imerg>). Hail measurements from the hailpad network in Croatia are available through inquiries of the Croatian Meteorological and Hydrological Service (usluge@cirus.dhz.hr) while radar products from Switzerland are available through data request at MeteoSwiss ([contact form](#)).

References

- Abatzoglou, J. T., & Williams, A. P. (2016). Impact of anthropogenic climate change on wildfire across Western US forests. *Proceedings of the National Academy of Sciences of the United States of America*, 113(42), 11770–11775. <https://doi.org/10.1073/PNAS.1607171113/-DCSUPPLEMENTAL>
- Adams-Selin, R. D., Clark, A. J., Melick, C. J., Dembek, S. R., Jirak, I. L., & Ziegler, C. L. (2019). Evolution of WRF-HAILCAST during the 2014-16 NOAA/hazardous weather testbed spring forecasting experiments. *Weather and Forecasting*, 34(1), 61–79. <https://doi.org/10.1175/WAF-D-18-0024.1>
- Adams-Selin, R. D., & Ziegler, C. L. (2016). Forecasting hail using a one-dimensional hail growth model within WRF. *Monthly Weather Review*, 144(12), 4919–4939. <https://doi.org/10.1175/MWR-D-16-0027.1>
- Allen, J. T., Giammanco, I. M., Kumjian, M. R., Jurgen Punge, H., Zhang, Q., Groenemeijer, P., et al. (2020). Understanding hail in the Earth system. *Reviews of Geophysics*, 58(Issue 1). <https://doi.org/10.1029/2019RG000665>
- Baldauf, M., Seifert, A., Förstner, J., Majewski, D., Raschendorfer, M., & Reinhardt, T. (2011). Operational convective-scale numerical weather prediction with the COSMO model: Description and sensitivities. *Monthly Weather Review*, 139(12), 3887–3905. <https://doi.org/10.1175/MWR-D-10-05013.1>
- Ban, N., Schmidli, J., & Schär, C. (2014). Evaluation of the convection-resolving regional climate modeling approach in decade-long simulations. *Journal of Geophysical Research*, 119(13), 7889–7907. <https://doi.org/10.1002/2014JD021478>
- Belušić, A., Prtenjak, M. T., Gütler, I., Ban, N., Leutwyler, D., & Schär, C. (2018). Near-surface wind variability over the broader Adriatic region: Insights from an ensemble of regional climate models. *Climate Dynamics*, 50(11–12), 4455–4480. <https://doi.org/10.1007/S00382-017-3885-5>
- Berthet, C., Dessens, J., & Sanchez, J. L. (2011). Regional and yearly variations of hail frequency and intensity in France. *Atmospheric Research*, 100(4), 391–400. <https://doi.org/10.1016/J.ATMOSRES.2010.10.008>
- Betz, H. D., Schmidt, K., Laroche, P., Blanchet, P., Oettinger, W. P., Defer, E., et al. (2009). LINET-An international lightning detection network in Europe [Dataset]. *Atmospheric Research*, 91(2–4), 564–573. <https://doi.org/10.1016/j.atmosres.2008.06.012>
- Brimelow, J. C., Reuter, G. W., & Poolman, E. R. (2002). Modeling maximum hail size in Alberta thunderstorms. *Weather and Forecasting*, 17(5), 1048–1062. [https://doi.org/10.1175/1520-0434\(2002\)017<1048:MMHSAI>2.0.CO;2](https://doi.org/10.1175/1520-0434(2002)017<1048:MMHSAI>2.0.CO;2)
- Brisson, E., Blahak, U., Lucas-Picher, P., Purr, C., & Ahrens, B. (2021). Contrasting lightning projection using the lightning potential index adapted in a convection-permitting regional climate model. *Climate Dynamics*, 1(7–8), 1–15. <https://doi.org/10.1007/S00382-021-05791-Z>
- Brisson, E., Brendel, C., Herzog, S., & Ahrens, B. (2018). Lagrangian evaluation of convective shower characteristics in a convection-permitting model. *MetZe*, 27(1), 59–66. <https://doi.org/10.1127/METZ/2017/0817>
- Brisson, E., Van Weverberg, K., Demuzere, M., Devis, A., Saeed, S., Stengel, M., & van Lipzig, N. P. M. (2016). How well can a convection-permitting climate model reproduce decadal statistics of precipitation, temperature and cloud characteristics? *Climate Dynamics*, 47(9–10), 3043–3061. <https://doi.org/10.1007/S00382-016-3012-Z>
- Brown, T. M., Pogorzelski, W. H., & Giammanco, I. M. (2015). Evaluating hail damage using property insurance claims data. *Weather, Climate, and Society*, 7(3), 197–210. <https://doi.org/10.1175/WCAS-D-15-0011.1>
- Changnon, S. A. (2009). Increasing major hail losses in the U.S. *Climatic Change*, 96(1), 161–166. <https://doi.org/10.1007/s10584-009-9597-z>
- Cui, R., Ban, N., Demory, M.-E., & Schär, C. (2023). Exploring hail and lightning diagnostics over the Alpine-Adriatic region in a km-scale climate model. *Weather and Climate Dynamics Discussions*, 1–31. <https://doi.org/10.5194/WCD-2023-11>
- Curran, E. B., Holle, R. L., & Lopez, R. E. (2000). Lightning casualties and damages in the United States from 1959 to 1994. *Journal of Climate*, 13(19), 3448–3464. [https://doi.org/10.1175/1520-0442\(2000\)013<3448:LCADIT>2.0.CO;2](https://doi.org/10.1175/1520-0442(2000)013<3448:LCADIT>2.0.CO;2)
- Czernecki, B., Taszarek, M., Marosz, M., Pórolniczak, M., Kolendowicz, L., Wyszogrodzki, A., & Szturc, J. (2019). Application of machine learning to large hail prediction - The importance of radar reflectivity, lightning occurrence and convective parameters derived from ERA5. *Atmospheric Research*, 227, 249–262. <https://doi.org/10.1016/j.atmosres.2019.05.010>
- Dessens, J. (1998). A physical evaluation of a hail suppression project with silver iodide ground burners in southwestern France. *Journal of Applied Meteorology*, 37(12), 1588–1599. [https://doi.org/10.1175/1520-0450\(1998\)037<1588:APEOAH>2.0.CO;2](https://doi.org/10.1175/1520-0450(1998)037<1588:APEOAH>2.0.CO;2)
- Dowdy, A. J., Fromm, M. D., & McCarthy, N. (2017). Pyrocumulonimbus lightning and fire ignition on Black Saturday in southeast Australia. *Journal of Geophysical Research: Atmospheres*, 122(14), 7342–7354. <https://doi.org/10.1002/2017JD026577>
- Ebert, E. E. (2008). Fuzzy verification of high-resolution gridded forecasts: A review and proposed framework. *Meteorological Applications*, 15(1), 51–64. <https://doi.org/10.1002/met.25>

Acknowledgments

This research is enabled by the SWAL-DRIC (IZHRZO-180587) project, which is financed within the Croatian-Swiss Research Program of the Croatian Science Foundation and the Swiss National Science Foundation with funds obtained from the Swiss-Croatian Cooperation Programme. Lightning data were obtained from the Lightning Detection Network in Europe (LINET) (<https://www.nowcast.de/en/solutions/linet-data>; 5 June 2022). Authors acknowledge MeteoSwiss for providing radar observations (POH), Croatian Meteorological and Hydrological Service for providing hailpad observations and NASA for providing IMERG data. ERA5 (Hersbach et al., 2020) was downloaded from the Copernicus Climate Change Service (C3S) Climate Data Store. The results contain modified Copernicus Climate Change Service information 2020. Neither the European Commission nor ECMWF is responsible for any use that may be made of the Copernicus information or data it contains. This research was supported by the WRF model (freely available at www.wrf-model.org/index.php). The WRF simulations were run using Isabella cluster (<https://www.srce.unizg.hr/en/>). RC, PV, NB, MED and CS acknowledge the Partnership for advanced computing in Europe (PRACE) for awarding access to Piz Daint at ETH Zürich at the Swiss National Supercomputing Centre (CSCS, Switzerland). The authors also acknowledge the Federal Office for Meteorology and Climatology (MeteoSwiss), CSCS, the Center for Climate Systems Modeling (C2SM) and ETH Zürich for their contributions to the development and maintenance of the GPU-accelerated version of COSMO. The anonymous reviewers are gratefully acknowledged for their in-depth review and valuable suggestions.

- Federer, B., Schmid, W., & Waldvogel, A. (1978). The design of Grossversuch IV, a randomized hail suppression experiment in Switzerland. *Atmosphere-Ocean*, 16(1), 6–16. <https://doi.org/10.1080/07055900.1978.9649009>
- Ferro, C. A. T., & Stephenson, D. B. (2011). Extremal dependence indices: Improved verification measures for deterministic forecasts of rare binary events. *Weather and Forecasting*, 26(5), 699–713. <https://doi.org/10.1175/WAF-D-10-05030.1>
- Foote, G. A., Krauss, T. W., & Makitov, V. (2005). Hail metrics using convectional radar. In *Proceedings of the 16th conference on planned and inadvertent weather modification*.
- Fowler, H. J., Ali, H., Allan, R. P., Ban, N., Barbero, R., Berg, P., et al. (2021). Towards advancing scientific knowledge of climate change impacts on short-duration rainfall extremes. *Philosophical Transactions of the Royal Society A: Mathematical, Physical & Engineering Sciences*, 379(2195), 20190542. <https://doi.org/10.1098/rsta.2019.0542>
- Franc, B., Filipović-Grčić, B., & Milardić, V. (2016). Lightning overvoltage performance of 110 kV air-insulated substation. *Electric Power Systems Research*, 138, 78–84. <https://doi.org/10.1016/j.epsr.2015.12.002>
- Germann, U., Boschetti, M., Gabella, M., & Sartori, M. (2015). Radar design for prediction in the Swiss Alps. *Meteorological Technology International*, 4, 42–45.
- Giaiotti, D., Nordio, S., & Stel, F. (2003). The climatology of hail in the plain of Friuli Venezia Giulia. *Atmospheric Research*, 67–68, 247–259. [https://doi.org/10.1016/S0169-8095\(03\)00084-X](https://doi.org/10.1016/S0169-8095(03)00084-X)
- Hentgen, L., Ban, N., Kröner, N., Leutwyler, D., & Schär, C. (2019). Clouds in convection-resolving climate simulations over Europe. *Journal of Geophysical Research: Atmospheres*, 124(7), 3849–3870. <https://doi.org/10.1029/2018JD030150>
- Hersbach, H., Bell, B., Berrisford, P., Hirahara, S., Horányi, A., Muñoz-Sabater, J., et al. (2020). The ERA5 global reanalysis. [Dataset]. *Quarterly Journal of the Royal Meteorological Society*, 146(730), 1999–2049. <https://doi.org/10.1002/qj.3803>
- Holle, R. L., López, R. E., & Navarro, B. C. (2005). Deaths, injuries, and damages from lightning in the United States in the 1890s in comparison with the 1990s. *Journal of Applied Meteorology and Climatology*, 44(10), 1563–1573. <https://doi.org/10.1175/JAM2287.1>
- Hong, S.-Y., & Lim, J.-O. J. (2006). The WRF single-moment 6-class microphysics scheme (WSM6). *Journal of the Korean Meteorological Society*, 42, 129–151.
- Horvath, K., Koracin, D., Vellere, R., Jiang, J., & Belu, R. (2012). Sub-kilometer dynamical downscaling of near-surface winds in complex terrain using WRF and MM5 mesoscale models. *Journal of Geophysical Research*, 117(11). <https://doi.org/10.1029/2012JD017432>
- Huffman, G. J., Bolvin, D. T., Braithwaite, D., Hsu, K., Joyce, R., Kidd, C., et al. (2019). NASA Global Precipitation Measurement (GPM) Integrated Multi-satellite Retrievals for GPM (IMERG) prepared for: Global precipitation measurement (GPM) National Aeronautics and Space Administration (NASA). Retrieved from https://pmm.nasa.gov/sites/default/files/imce/times_allsat.jpg
- Jelić, D., Megyeri, O. A., Malečić, B., Belušić Vozila, A., Strelec Mahović, N., & Prtenjak, M. T. (2020). Hail climatology along the Northeastern Adriatic. *Journal of Geophysical Research: Atmospheres*, 125(23). <https://doi.org/10.1029/2020JD032749>
- Jelić, D., Prtenjak, M. T., Malečić, B., Vozila, A. B., Megyeri, O. A., & Renko, T. (2021). A new approach for the analysis of deep convective events: Thunderstorm intensity index. *Atmosphere*, 12(7), 908. <https://doi.org/10.3390/ATMOS12070908>
- Jewell, R., & Brimelow, J. (2009). Evaluation of Alberta hail growth model using severe hail proximity soundings from the United States. *Weather and Forecasting*, 24(6), 1592–1609. <https://doi.org/10.1175/2009WAF2222230.1>
- Joe, P., Burgess, D., Potts, R., Keenan, T., Stumpf, G., & Treloar, A. (2004). The S2K severe weather detection algorithms and their performance. *Weather and Forecasting*, 19(1), 43–63. [https://doi.org/10.1175/1520-0434\(2004\)019<0043:TSSWDA>2.0.CO;2](https://doi.org/10.1175/1520-0434(2004)019<0043:TSSWDA>2.0.CO;2)
- Kain, J. S., & Kain, J. (2004). The Kain - Fritsch convective parameterization: An update. *Journal of Applied Meteorology*, 43(1), 170–181. [https://doi.org/10.1175/1520-0450\(2004\)043<0170:TKCPAU>2.0.CO;2](https://doi.org/10.1175/1520-0450(2004)043<0170:TKCPAU>2.0.CO;2)
- Kanata, J., Ametani, A., & Yamamoto, K. (2012). Threats of lightning current through an electric vehicle. 2012 31st International Conference on Lightning Protection. ICLP 2012. <https://doi.org/10.1109/ICLP.2012.6344299>
- Keller, M., Fuhrer, O., Schmidli, J., Stengel, M., Stöckli, R., & Schär, C. (2016). Evaluation of convection-resolving models using satellite data: The diurnal cycle of summer convection over the Alps. *Meteorologische Zeitschrift*, 25(2), 165–179. <https://doi.org/10.1127/METZ/2015/0715>
- Klasa, C., Arpagaus, M., Walser, A., & Wernli, H. (2018). An evaluation of the convection-permitting ensemble COSMO-E for three contrasting precipitation events in Switzerland. *Quarterly Journal of the Royal Meteorological Society*, 144(712), 744–764. <https://doi.org/10.1002/qj.3245>
- Kunz, M., Blahak, U., Handwerker, J., Schmidberger, M., Punge, H. J., Mohr, S., et al. (2018). The severe hailstorm in southwest Germany on 28 July 2013: Characteristics, impacts and meteorological conditions. *Quarterly Journal of the Royal Meteorological Society*, 144(710), 231–250. <https://doi.org/10.1002/qj.3197>
- Lagasio, M., Parodi, A., Procopio, R., Rachidi, F., & Fiori, E. (2017). Lightning potential index performances in multimicrophysical cloud-resolving simulations of a back-building mesoscale convective system: The Genoa 2014 event. *Journal of Geophysical Research*, 122(8), 4238–4257. <https://doi.org/10.1002/2016JD026115>
- Latham, D., & Williams, E. (2001). Lightning and forest fires. *Forest Fires*, 375–418. <https://doi.org/10.1016/B978-012386660-8/50013-1>
- Lavin-Gullon, A., Fernandez, J., Bastin, S., Cardoso, R. M., Fita, L., Giannaros, T. M., et al. (2021). Internal variability versus multi-physics uncertainty in a regional climate model. *International Journal of Climatology*, 41(S1), E656–E671. <https://doi.org/10.1002/joc.6717>
- Lee, J. Y., & Collins, G. J. (2017). Risk analysis of lightning effects in aircraft systems. *IEEE Aerospace Conference Proceedings*. <https://doi.org/10.1109/AERO.2017.7943671>
- Leutwyler, D., Lüthi, D., Ban, N., Fuhrer, O., & Schär, C. (2017). Evaluation of the convection-resolving climate modeling approach on continental scales. *Journal of Geophysical Research: Atmospheres*, 122(10), 5237–5258. <https://doi.org/10.1002/2016JD026013>
- Lynn, B., & Yair, Y. (2010). Prediction of lightning flash density with the WRF model. *Advances in Geosciences*, 23(February), 11–16. <https://doi.org/10.5194/adgeo-23-11-2010>
- Malečić, B., Prtenjak, M. T., Horvath, K., Jelić, D., Jurković, P. M., Čorko, K., & Mahović, N. S. (2022). Performance of HAILCAST and the lightning potential index in simulating hailstorms in Croatia in a mesoscale model – Sensitivity to the PBL and microphysics parameterization schemes. *Atmospheric Research*, 272(March), 106143. <https://doi.org/10.1016/j.atmosres.2022.106143>
- Manzato, A. (2012). Hail in Northeast Italy: Climatology and bivariate analysis with the sounding-derived indices. *Journal of Applied Meteorology and Climatology*, 51(3), 449–467. <https://doi.org/10.1175/JAMC-D-10-05012.1>
- Manzato, A., Riva, V., Tiesi, A., & Marcello Miglietta, M. (2020). Observational analysis and simulations of a severe hailstorm in northeastern Italy. *Quarterly Journal of the Royal Meteorological Society*, 146(732), 3587–3611. <https://doi.org/10.1002/qj.3886>
- Mlawer, E. J., Taubman, S. J., Brown, P. D., Iacono, M. J., & Clough, S. A. (1997). Radiative transfer for inhomogeneous atmospheres: RRTM, a validated correlated-k model for the longwave. *Journal of Geophysical Research*, 102(14), 16663–16682. <https://doi.org/10.1029/97jd00237>
- Morel, S. (2014). Verification of radar-based hail detection algorithms with insurance loss data in Switzerland, (MS thesis). University of Bern (p.83).

- Nakanishi, M., & Niino, H. (2006). An improved Mellor-Yamada Level-3 model: Its numerical stability and application to a regional prediction of advection fog. *Boundary-Layer Meteorology*, *119*(2), 397–407. <https://doi.org/10.1007/s10546-005-9030-8>
- Nisi, L., Martius, O., Hering, A., Kunz, M., & Germann, U. (2016). Spatial and temporal distribution of hailstorms in the Alpine region: A long-term, high resolution, radar-based analysis. *Quarterly Journal of the Royal Meteorological Society*, *142*(697), 1590–1604. <https://doi.org/10.1002/qj.2771>
- Park, S. H., Skamarock, W. C., Klemp, J. B., Fowler, L. D., & Duda, M. G. (2013). Evaluation of global atmospheric solvers using extensions of the Jablonowski and Williamson baroclinic wave test case. *Monthly Weather Review*, *141*(9), 3116–3129. <https://doi.org/10.1175/MWR-D-12-00096.1>
- Pichelli, E., Coppola, E., Sobolowski, S., Ban, N., Giorgi, F., Stocchi, P., et al. (2021). The first multi-model ensemble of regional climate simulations at kilometer-scale resolution part 2: Historical and future simulations of precipitation. *Climate Dynamics*, *56*(11–12), 3581–3602. <https://doi.org/10.1007/s00382-021-05657-4>
- Počakal, D. (2011). Hailpad data analysis for the continental part of Croatia. *Meteorologische Zeitschrift*, *20*(4), 441–447. <https://doi.org/10.1127/0941-2948/2011/0263>
- Počakal, D., Večenaj, Ž., Mikuš Jurković, P., & Grisogono, B. (2018). Analysis of orographic influence on hail parameters in NW Croatia. *International Journal of Climatology*, *38*(15), 5646–5658. <https://doi.org/10.1002/joc.5769>
- Počakal, D., Večenaj, Ž., & Štalcic, J. (2009). Hail characteristics of different regions in continental part of Croatia based on influence of orography. *Atmospheric Research*, *93*(1–3), 516–525. <https://doi.org/10.1016/j.atmosres.2008.10.017>
- Poolman, E. R. (1992). *Die voorspelling van haelkorrelgroei in Suid-Afrika (The forecasting of hail growth in South Africa)*. MS thesis. Faculty of Engineering University of Pretoria.
- Prein, A. F., Holland, G. J., Rasmussen, R. M., Done, J., Ikeda, K., Clark, M. P., & Liu, C. H. (2013). Importance of regional climate model grid spacing for the simulation of heavy precipitation in the Colorado headwaters. *Journal of Climate*, *26*(13), 4848–4857. <https://doi.org/10.1175/JCLI-D-12-00727.1>
- Púčik, T., Castellano, C., Groenemeijer, P., Kühne, T., Rädler, A. T., Antonescu, B., & Faust, E. (2019). Large hail incidence and its economic and societal impacts across Europe. *Monthly Weather Review*, *147*(11), 3901–3916. <https://doi.org/10.1175/MWR-D-19-0204.1>
- Punge, H. J., & Kunz, M. (2016). Hail observations and hailstorm characteristics in Europe: A review. *Atmospheric Research*, *176–177*, 159–184. <https://doi.org/10.1016/j.atmosres.2016.02.012>
- Rachidi, F., Rubinstein, M., Montanyà, J., Bermúdez, J. L., Sola, R. R., Solà, G., & Korovkin, N. (2008). A review of current issues in lightning protection of new-generation wind-turbine blades. *IEEE Transactions on Industrial Electronics*, *55*(6), 2489–2496. <https://doi.org/10.1109/TIE.2007.896443>
- Raschendorfer, M. (2001). The new turbulence parameterization of LM. *COSMO Newsletter*, *1*, 89–97. Retrieved from http://www.joi.isoss.net/PDFs/Vol-7-no-2-2021/03_J_ISOSS_7_2.pdf
- Raupach, T. H., Martynov, A., Nisi, L., Hering, A., Barton, Y., & Martius, O. (2021). Object-based analysis of simulated thunderstorms in Switzerland: Application and validation of automated thunderstorm tracking on simulation data. May, 1–29. *Geoscientific Model Development Discussions*. <https://doi.org/10.5194/gmd-2021-105>
- Ritter, B., & Geleyn, J. F. (1992). A comprehensive radiation scheme for numerical weather prediction models with potential applications in climate simulations. *Monthly Weather Review*, *120*(2), 303–325. [https://doi.org/10.1175/1520-0493\(1992\)120<0303:acrsfn>2.0.co;2](https://doi.org/10.1175/1520-0493(1992)120<0303:acrsfn>2.0.co;2)
- Romps, D. M., Seeley, J. T., Vollaro, D., & Molinari, J. (2014). Projected increase in lightning strikes in the United States due to global warming. *Science*, *346*(6211), 851–854. <https://doi.org/10.1126/science.1259100>
- Schär, C., Fuhrer, O., Arteaga, A., Ban, N., Charpiroz, C., Di Girolamo, S., et al. (2020). Kilometer-scale climate models: Prospects and challenges. *Bulletin of the American Meteorological Society*, *101*(5), E567–E587. <https://doi.org/10.1175/BAMS-D-18-0167.1>
- Schuster, S. S., Blong, R. J., Leigh, R. J., & McAneney, K. J. (2005). April 1999 Sydney hailstorm based on ground observations, weather radar, insurance data and emergency calls. *Natural Hazards and Earth System Sciences*, *5*(5), 613–620. <https://doi.org/10.5194/nhess-5-613-2005>
- Sioutas, M., Meaden, T., & Webb, J. D. C. (2009). Hail frequency, distribution and intensity in Northern Greece. *Atmospheric Research*, *93*(1–3), 526–533. <https://doi.org/10.1016/j.atmosres.2008.09.023>
- Skamarock, C., Klemp, B., Dudhia, J., Gill, O., Liu, Z., Berner, J., et al. (2019). A description of the advanced research WRF model version 4. *NCAR Technical Notes*. <https://doi.org/10.5065/1DFH-6P97>
- Skamarock, W. C. (2004). Evaluating mesoscale NWP models using kinetic energy spectra. *Monthly Weather Review*, *132*(12), 3019–3032. <https://doi.org/10.1175/MWR2830.1>
- Smith, P. L., & Waldvogel, A. (1989). On determinations of maximum hailstone sizes from hailpad observations. *Journal of Applied Meteorology*, *28*(1), 71–76. [https://doi.org/10.1175/1520-0450\(1989\)028<0071:odomhs>2.0.co;2](https://doi.org/10.1175/1520-0450(1989)028<0071:odomhs>2.0.co;2)
- Sokol, Z., & Minářová, J. (2020). Impact of 1- and 2-moment cloud microphysics and horizontal resolution on lightning potential index within COSMO NWP model. *Atmospheric Research*, *237*, 104862. <https://doi.org/10.1016/j.atmosres.2020.104862>
- Svabik, O. (1989). Review of meteorological aspects on hail defense activities in Austria. *Theoretical and Applied Climatology*, *40*(4), 247–254. <https://doi.org/10.1007/BF00865975>
- Taylor, K. E. (2001). Summarizing multiple aspects of model performance in a single diagram. *Journal of Geophysical Research*, *106*(D7), 7183–7192. <https://doi.org/10.1029/2000JD900719>
- Thornton, J. A., Virts, K. S., Holzworth, R. H., & Mitchell, T. P. (2017). Lightning enhancement over major oceanic shipping lanes. *Geophysical Research Letters*, *44*(17), 9102–9111. <https://doi.org/10.1002/2017GL074982>
- Tiedtke, M. (1989). A comprehensive mass flux scheme for cumulus parameterization in large-scale models. *Monthly Weather Review*, *117*(8), 1779–1800. [https://doi.org/10.1175/1520-0493\(1989\)117<1779:ACMFSF>2.0.CO;2](https://doi.org/10.1175/1520-0493(1989)117<1779:ACMFSF>2.0.CO;2)
- Tiesi, A., Mazzà, S., Conte, D., Ricchi, A., Baldini, L., Montopoli, M., et al. (2022). Numerical simulation of a Giant-hail-bearing Mediterranean supercell in the Adriatic Sea. *Atmosphere*, *13*(8), 1219. <https://doi.org/10.3390/ATMOS13081219>
- Trefalt, S., Martynov, A., Barras, H., Besic, N., Hering, A. M., Lenggenhager, S., et al. (2018). A severe hail storm in complex topography in Switzerland - observations and processes. *Atmospheric Research*, *209*, 76–94. <https://doi.org/10.1016/j.atmosres.2018.03.007>
- Treloar, A. B. A. (1998). Vertically integrated radar reflectivity as an indicator of hail size in the greater Sydney region of Australia. In *19th conference on severe local storms* (p. 3).
- Vergara-Temprado, J., Ban, N., Panosetti, D., Schlemmer, L., & Schär, C. (2020). Climate models permit convection at much coarser resolutions than previously considered. *Journal of Climate*, *33*(5), 1915–1933. <https://doi.org/10.1175/JCLI-D-19-0286.1>
- Vergara-Temprado, J., Ban, N., & Schär, C. (2021). Extreme sub-hourly precipitation intensities scale close to the Clausius-Clapeyron rate over Europe. *Geophysical Research Letters*, *48*(3). <https://doi.org/10.1029/2020GL089506>

- Waldvogel, A., Federer, B., & Grimm, P. (1979). Criteria for detection of hail cells. *Journal of Applied Meteorology*, *18*(12), 1521–1525. [https://doi.org/10.1175/1520-0450\(1979\)018<1521:CFTDOH>2.0.CO;2](https://doi.org/10.1175/1520-0450(1979)018<1521:CFTDOH>2.0.CO;2)
- Willemse, S., & Furger, M. (2016). From weather observations to atmospheric and climate sciences in Switzerland. Celebrating 100 years of the Swiss Society of Meteorology.
- Witt, A., Eilts, M. D., Stumpf, G. J., Johnson, J. T., Mitchell, E. D., & Thomas, K. W. (1998). An enhanced hail detection algorithm for the WSR-88D. *Weather and Forecasting*, *13*(2), 286–303. [https://doi.org/10.1175/1520-0434\(1998\)013<0286:AEHDAF>2.0.CO;2](https://doi.org/10.1175/1520-0434(1998)013<0286:AEHDAF>2.0.CO;2)
- Yair, Y., Lynn, B., Price, C., Kotroni, V., Lagouvardos, K., Morin, E., et al. (2010). Predicting the potential for lightning activity in Mediterranean storms based on the Weather Research and Forecasting (WRF) model dynamic and microphysical fields. *Journal of Geophysical Research*, *115*(4), D04205. <https://doi.org/10.1029/2008JD010868>
- Zeman, C., Wedi, N. P., Dueben, P. D., Ban, N., & Schär, C. (2021). Model intercomparison of COSMO 5.0 and IFS 45r1 at kilometer-scale grid spacing. *Geoscientific Model Development*, *14*(7), 1–23. <https://doi.org/10.5194/gmd-14-4617-2021>

References From the Supporting Information

- Kain, J. S., Weiss, S. J., Levit, J. J., Baldwin, M. E., & Bright, D. R. (2006). Examination of convection-allowing configurations of the WRF model for the prediction of severe convective weather. The SPC/NSSL Spring Program 2004.
- Lynn, B. H., & Yair, Y. Y. (2008). Lightning power index: A new tool for predicting the lightning density and the potential for extreme rainfall. In *Geophysical research abstracts* (Vol. 10).
- Saunders, C. (2008). Charge separation mechanisms in clouds. *Space Science Reviews*, *137*(1–4), 335–353. <https://doi.org/10.1007/s11214-008-9345-0>
- Weisman, M. L., Skamarock, W. C., & Klemp, J. B. (1997). The resolution dependence of explicitly modeled convective systems. *Monthly Weather Review*, *125*(4), 527–548. [https://doi.org/10.1175/1520-0493\(1997\)125<0527:TRDOEM>2.0.CO;2](https://doi.org/10.1175/1520-0493(1997)125<0527:TRDOEM>2.0.CO;2)